From the Department of Medicine, Karolinska Institutet,
Division of Nuclear Medicine, Department of Surgical Science,
Karolinska Institutet and
Division of Surgery, Karolinska Institutet Danderyd Hospital,
Stockholm, Sweden

Imaging-based dynamic liver testing

Studies of segmental hepatic parenchymal function and biliary flow using dynamic $^{99}Tc^{m}$-HIDA SPECT

Eduard Jonas

Leg. Läkare

Stockholm 2002

Published and printed by Karolinska University Press
Box 200, SE-171 77 Stockholm, Sweden

ISBN 91-7349-376-7

“La race humaine veut des idées simples. Or le réel est compliqué”
Claude Couinaud

ABSTRACT

The aim of the study was to create a dynamic liver function test using a tomographic imaging procedure as sampling method. The liver has multiple and complex functions. It is obvious that no single test can give a comprehensive measurement of total liver function. Currently available tests, including analyte measurements and clearance tests, give limited information. Furthermore, no test is able to measure function on a segmental level. The ultimate liver function test is probably multi-compartment quantitative analysis (QA) of a dynamic test. This requires a safe, well tolerated test substance, not influenced by diet, drugs or genetic factors. As a dynamic test requires repetitive sampling, the sampling method should be non-invasive and able to detect the test substance in all compartments involved in the kinetics of the test substance.

We have developed a technique of dynamic $^{99}Tc^{m}$-HIDA SPECT (single photon emission computed tomography) allowing creation of time-activity curves for the isotope in individual liver segments. QA of these curves can measure uptake and excretion of the isotope as an indication of function on a segmental level. In principle, the test is a dynamic liver function test using an imaging modality (SPECT) as sampling device.

The concept was simulated in a 3-D virtual reality liver model. Advancing the dynamic SPECT technique according to the model, we separated activity for parenchyma and bile ducts and created separate dynamic studies for these structures.

This refinement, being a step in the direction of a true multi-compartmental dynamic test, using image sampling, was tested in a normal volunteer population and in patients with primary sclerosing cholangitis (PSC). The complicated management of PSC stresses the limitations of currently used liver function tests. In patients with PSC, QA of the dynamic SPECT data correlated statistically significantly with biochemical parameters and the revised Mayo prognostic score. On a segmental level, the scintigraphic data reflecting biliary flow correlated with cholangiographic findings.

A method capable of evaluating liver function and quantifying bile flow on a segmental level has several possible applications, particularly in segmental liver diseases. It may aid in predicting prognosis and selecting and timing of various treatment options. Specifically, the importance of radiologically detected strictures in terms of flow obstruction can be quantified and the outcome of intervention measured.

Our data suggest differences in liver function between different segments in normal livers. Expressing total liver function as the total of the product of volume and segmental function in individual segments, may give a more accurate estimate of total liver function. Physiological differences between the left and right hemi-livers, as indicated by our results, may play a role in the non-homogeneity and hemi-liver preferences of some liver diseases.

LIST OF PUBLICATIONS

The thesis is based on the following papers, which will be referred to in the text by their roman numbers:

I. Jonas E, Hultcrantz R, Slezak P, Blomqvist L, Schnell P-O, Jacobsson H. Dynamic $^{99}Tc^{m}$-HIDA SPET: non-invasive measuring of intrahepatic bile flow. Description of the method and a study in primary sclerosing cholangitis. Nucl Med Commun. 2001;22:127-34

II. Jonas E, Slezak P, Miller N. Imaging-based dynamic liver testing - a computerised simulation. Hepatogastroenterology. 2000;47:967-72

III. Jonas E, Hultcrantz R, Näslund E, Freedman J, Slezak P, Jacobsson H. Separation of hepatic parenchymal and intrahepatic bile duct isotope activity: Dynamic studies of parenchymal function and bile duct flow using dynamic $^{99}Tc^{m}$-HIDA SPECT. World Journal of Nuclear Medicine. In press

IV. Jonas E, Näslund E, Freedman J, Befrits R, Blomqvist L, Sjösteen A-C, Jacobsson H, Hultcrantz R. Parenchymal function and bile duct flow in primary sclerosing cholangitis using dynamic $^{99}Tc^{m}$-HIDA SPECT. A comparative study with the Mayo natural history model and cholangiographic findings. Manuscript

V. Jacobsson H, Jonas E, Hellström PM, Larsson SA. Concentrations of [^{123}I]-MIBG, $^{99}Tc^{m}$-anti-granulocyte antibody, ^{111}In-pentetreotide and $^{99}Tc^{m}$-HIDA in the left and right hemi-livers. Scintigraphy indicating regional functional differences in the normal liver. Manuscript

Reprinted with permission from Lippincott Williams & Wilkins, Baltimore, USA (I); H.G.E. Update Medical Publishing, S.A., Athens, Greece (II) and World Journal of Nuclear Medicine, Vienna, Austria (III)

CONTENTS

LIST OF ABBREVIATIONS

3-D	three-dimensional
ALP	alkaline phosphatase
ALT	alanine aminotransferase
AST	aspartate aminotransferase
BSP	bromsulphthalein
CCAS	cranio-caudal activity scanning
CCDS	cranio-caudal density scanning
C_{max}	peak counts
CT	computed tomography
D_{max}	peak density
Dt_{max}	time point at peak density
ERCP	endoscopic retrograde cholangio-pancreatography
excretion $Dt_{½}$	time after which density decreased to 50 % of D_{max}
excretion $t_{½}$	time after which counts decreased to 50 % of C_{max}
Gd-EoB-DTPA	gadolinium ethoxybenzyl diethylenetriaminepentaacetic acid
GGT	gamma glutamyl transpeptidase
GSA	galactosyl-human serum albumin
HIDA	hepatic N-(2,6 diethylphenylcarbomoylmethyl) iminodiacetic acid
IBD	inflammatory bowel disease
ICG	indocyanine green
MEGX	mono-ethyl-glycine-xylidide
MIBG	metaiodobenzylguanidine
Mn-DPDP	mangafodipir
MoAb	monoclonal antibody against granulocytes
MR	magnetic resonance
MRCP	magnetic resonance cholangio-pancreatography
PSC	primary sclerosing cholangitis
QA	quantitative analysis
ROI	region of interest
SPECT	single photon emission computed tomography
t_{max}	time point at peak counts
UDCA	ursodeoxycholic acid
VOI	volume of interest

1 INTRODUCTION

The liver has been associated with human qualities, some admired, some detested. To Goneril, King Lear's eldest daughter, her husband, the Duke of Albany whom she regarded as a coward, was a "milk-livered man". "Umntu onesibindi" (a person with liver) is the term for a courageous person among the Xhosa from eastern South Africa. In Babylonian antiquity the liver was studied to forecast the future. Babylonian priests in ancient Mesopotamian predicted the outcome of events using the pseudo-science of "hepatoscopy". Their rules are known from the discovery of ancient clay models of the liver with its several lobes, each part being inscribed with its significance according to its appearance (1). The liver's central importance in the functioning of the human body was clear since early times, albeit for the wrong reasons. "Now why is the stomach surrounded by the liver? Is it in order that the liver may warm it and it may in turn warm the food? This is indeed the very reason why it is closely clasped by the lobes of the liver, as if by fingers", wrote Galen, ca 200 A.D. He propagated the liver as "the source of the veins and the principal instrument of sanguification". These views reigned largely unchanged and unchallenged into the 17th century. In his classical work on the lymphatic system, the Danish anatomist, Thomas Bartholin declared the end of the liver's role as "ruler of the abdomen" and the "death of the sanguine empire" (2). Although the liver had to abdicate some of its earlier claimed functions to their rightful owners, it maintains its position as executioner of some of the most complex biological functions in the human body.

1.1 EMBRYOLOGY

The liver develops as a ventral outgrowth of the foregut as a rapidly dividing mass of cells invading the septum transversum and two sets of longitudinal veins (vitelline and umbilical veins) (Figure 1). The hepatic vascular and biliary development can be divided into four stages (3):

1. *Venous invasion*
The developing liver invades the left and right vitelline veins, running from the gut-yolk sac complex to the heart. The middle section of the vein capilarizes, whereas the caudal and cranial ends persist as the primitive portal and hepatic veins respectively. This results in division of the developing liver into a left and right side based on a vascular watershed. In adult life this division persists as separate portal and hepatic arterial circulations. At a later stage during embryological development the left umbilical vein is invaded by the developing liver. With time all umbilical venous blood will pass through the liver.

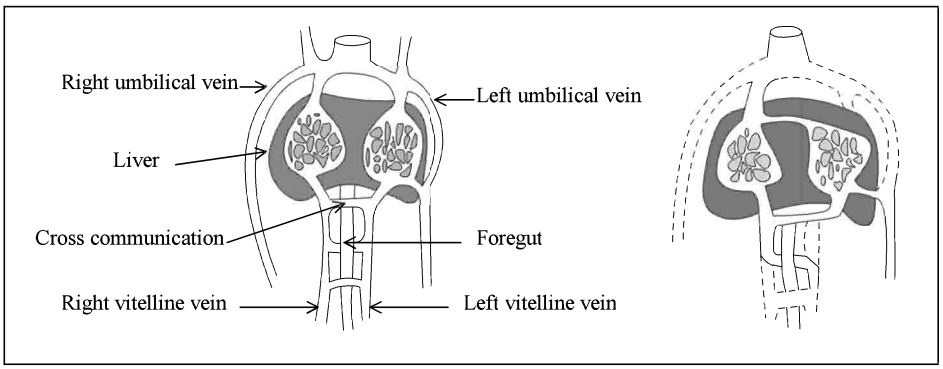

Figure 1. *Embryological development of the liver*

2. *Vein regression*
During this stage the entire right umbilical vein and cranial part of the left umbilical vein obliterate. Parts of the caudal vitelline veins, including the part of the left vein closest to the liver, the lowest cross-communication between the left and right vitelline veins and right vitelline vein caudal to the middle cross-communication regresses. The middle cross-communication becomes the part of the portal vein running posterior of the duodenum while the upper cross-communication becomes the origin of the left portal vein running inferior in segment IV. The main portal vein is derived from the right vitelline vein and the middle cross-communication. The cranial part of the left vitelline vein obliterates whereas the right part is incorporated into the inferior vena cava.

3. *New vein formation*
The left and middle hepatic veins are formed by consolidation of smaller channels of predominantly the left vitelline system, whereas the right hepatic vein is a branch of the original right vitelline vein. The ductus venosis develops from elements of the vitelline system as a shunt between the left umbilical vein and common hepatic vein. At birth the extrahepatic portions of the umbilical vein and the ductus venosis obliterate to form the ligamentum teres and ligamentum venosum. The hepatic part of the umbilical vein persists as

the umbilical portion of the left portal vein. In contrast to the right portal system, that is formed from the right vitelline system, both the left umbilical and vitelline veins contribute to the formation of the left portal system. At birth reversal of flow occurs in the umbilical portion of the left portal vein, changing it from a placenta to heart conduit in foetal life to a gut to liver conduit in postnatal life.

4. *Artery and bile duct formation*
Formation of arteries and bile ducts occurs much later during intra-uterine life. Growth is along the already formed portal structures with one important exception in the left liver. On the left side the arteries and ducts follow the first part of the portal vein up to the umbilical part where it divides into two equal branches, supplying and draining the left-sided hepatic tissue on the right (segment IV) and left (segment II and III) of the umbilical recess.

The blood supply of the left and right hemi-livers differs during foetal life. The left hemi-liver receives exclusively placental blood, whereas the right hemi-liver receives both placental blood and blood returning through the foetal portal system. Portal venous blood contains hepatotrophic substances, including insulin, glucagon and hepatocyte growth factor (HGF) (4-6). During foetal life only the developing right hemi-liver is exposed to these substances on first pass. This is likely to result in differences between the development of left- and right-sided hepatocytes. The switch from placental to portal circulation and reversal in flow in a portion of the portal vein occurring in the left portal system at birth is a unique event in the body.

1.2 ANATOMY

The liver can be described according to morphological anatomy or functional anatomy (Figure 2) (7). Morphologically the umbilical fissure and falciform ligament divide the liver in a large right and smaller left lobe. The transverse hilar fissure divides the part of the right lobe between the gallbladder fossa and the umbilical fissure in an anterior quadrate lobe and posterior caudate lobe. The small Spigelian lobe is situated posterior of the caudate lobe. This lobar classification, based on features observed on the surface of the liver, is misleading and non-functional as far as physiology and surgery of the liver are concerned (7).

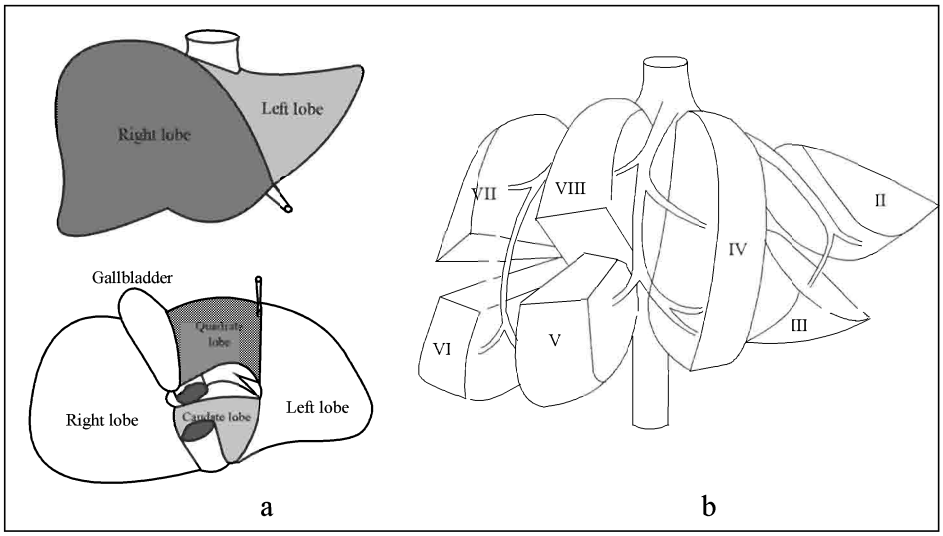

Figure 2. *Morphological (a) and functional segmental (b) anatomy of the liver*

Cantlie showed with ink injection in the hepatic inflow vessels and bile ducts that the principal division of the liver is based on a vascular watershed lying in the vertical plane intersecting the gallbladder fossa and inferior vena cava (8). Work by McIndoe and Councellor, Hjortsjö and Healey and Schroy has contributed to the development of the segmental concept of the liver (9-11). The currently accepted segmental classification of liver anatomy is largely based on work of Couinaud and forms the scientific basis for segmental liver resections (12, 13). As far as nomenclature of segmental liver anatomy is concerned, we adhere to the system proposed by Strasberg (14).

The liver is divided into 8 functionally independent segments, numbered I to VIII (Figure 2b). The segments, with the exception of segment I, are defined by one horizontal and three vertical planes. The vertical planes correspond to planes formed by the right and middle hepatic veins and umbilical fissure/falciform ligament. The vertical plane runs on the level of the left and right portal veins. Segment I deviates from the segmental concept concerning blood supply and venous and biliary drainage. Segments II-VIII are divided into 4 sectors, in the right hemi-liver a posterior (segments VI and VII) and anterior (segments V and VIII) sector and in the left hemi-liver a medial (segment IV) and lateral (segments II and III) sector.

1.3 LIVER FUNCTION TESTS

The functions of the liver are multiple and complex, including synthesis and storage, secretion, excretion, detoxification and the metabolising of nutrients, hormones and drugs. These functions are maintained by a complex integration of cellular processes dependent on an adequate blood supply, the functional integrity of the parenchymal mass and effective drainage capacity of the bile ducts and hepatic veins. It is obvious that no single test can measure total liver function. Currently available tests of liver function can roughly be divided into simple analyte measurements and clearance tests.

Analyte measurements
Their ease of performance and low cost make analyte tests the most commonly used measures of hepatic function in clinical practice. They give indirect indications of liver function and include measurements of cell permeability or damage (liver enzymes), synthetic capability (coagulation parameters and albumin) and metabolic integrity (bilirubin) (15). These tests are used in isolation, or in combination in scoring systems like the Child-Pugh score (16). Most of the tests, however, are non-specific and serum levels are influenced by factors other than liver function.

Liver enzymes reflect damage of liver cells and the subsequent wash-out of enzymes (17). Serum levels of alkaline phosphatase (ALP) rise in cholestasis and to a lesser extent with parenchymal cell damage. It is not liver-specific and is known to rise with bone diseases. Raised levels, probably from bowel origin, are found in benign familial hyperphosphatasaemia (18). A rise in gamma-glutamyl transpeptidase (GGT), in association with ALP, indicates cholestasis. An isolated rise is often associated with alcohol abuse. The aminotransferases usually reflect hepatocellular damage. The serum levels of enzymes do however not always reflect the degree of hepatic failure. If one would remove the whole liver, enzyme levels would be normal or reduced despite the total absence of liver function.

Serum albumin levels and parameters of coagulation status are often used as measure of the synthetic capability of the liver. Approximately 10 % of the daily requirements of albumin are synthesised by the liver, the rest being acquired by dietary intake. Changes in serum albumin levels as result of parenchymal dysfunction lag behind the actual hepatocellular changes, as serum albumin has a half-life of 22 days. Malnutrition and renal or intestinal loss also influence levels. The liver is the principal site for the synthesis of all coagulation factors with the exception of Von Willebrand factor and factor VIIIC. Factors influencing the integrity of the coagulation capability are, however, multiple.

Both production and excretion influence bilirubin levels. Unconjugated levels may be increased in massive haemolysis in the absence of liver disease. Parenchymal damage usually gives rise to unconjugated bilirubin, whereas the conjugated fraction rises in the presence of biliary obstruction. Comparison of conjugated versus unconjugated fractions is too unreliable an indicator of level of disease to make it useful in clinical practice. Changes in bilirubin levels tend to lag behind actual changes in liver function by days.

Clearance tests
Clearance tests measure clearance of substrates from the blood and in some cases the formation of a substrate metabolite. A large variety of substances have been used, including

bromsulphthalein (BSP), lignocaine and its metabolite mono-ethyl-glycine-xylidide (MEGX), galactose, aminopyrine, caffeine, indocyanine green (ICG) and dextrometorphan (19-22). These tests are believed to be more accurate than analyte measurements but still give limited information, as the integrity of one, or at most a few enzymes is determined.

Intrinsic hepatic clearance approaches systemic clearance when the test substrate is primarily removed by the liver. Clearance is therefore a function of hepatic perfusion (Q) and hepatic functional capability. Functional capacity is expressed as excretion ratio (E) which is determined by the ratio of the difference between the inflow (C_i) and outflow (C_o) concentrations and inflow concentrations of the test substrate.

$$E = (C_i - C_o)/ C_i$$
$$\text{Clearance} = Q X E$$

Clearance of substances with high extraction ratios (>0.7), for example ICG, galactose and lignocaine is largely dependent on liver blood flow and only becomes dependent on liver metabolism at low perfusion states of the liver. In patients with advanced liver disease clearance becomes less dependent on perfusion. Comparison of mild and severe liver disease may therefore be inaccurate as one may be measuring different processes (19). Clearance of substances with low extraction ratios (<0.3), including antipyrine and caffeine, is largely independent of perfusion and gives a more true reflection of hepatic metabolic capacity (23). Clearance tests are cumbersome and are generally not used in daily clinical activities.

All of the above-mentioned tests are used as indicators of liver function for the hepatic unit as a whole. No test exists that can evaluate liver function on a regional or segmental level.

1.4 HEPATIC SCINTIGRAPHY

Emphasis in hepatic scintigraphy shifted from mainly morphological imaging in the pre-computed tomography (CT), magnetic resonance (MR) and ultrasound era to functional imaging. Building on the principle of clearance tests, it was a simple conceptual step to go from chemical measurements of a pharmacological tracer to measuring clearance of a radioactive tracer. ^{131}I-Rose Bengal, a radioactive derivative of BSP, was initially used with radioassay of blood samples (24, 25). The logical next step was to replace blood sampling with external counting with a gamma camera. This offered the advantage of detection of the tracer not only in the blood pool, but also in the liver and bowel. Early attempts at scintigraphic measurement of hepatocellular function were frustrated by the quality of available pharmaceuticals. ^{131}I-Rose Bengal, was liver-specific but had slow hepatic clearance and poor physical qualities (24-28).

The development of ^{99}Tc^{m}-labelled hepatic N-(2,6 diethylphenylcarbomoylmethyl) iminodiacetic acid (HIDA) by Loberg and co-workers in 1976 was a major advance (29). Hepatic uptake of the ^{99}Tc^{m}-HIDA deriverates varies from a low of 82.5 % for the earlier substances to 98 % for new generation substances like ^{99}Tc^{m}-mebrofenin (30). ^{99}Tc^{m}-HIDA agents are transported in blood, bound to serum albumin as an albumin-^{99}Tc^{m}-HIDA complex. Disassociation of the complex takes place in the space of Disse after which the ^{99}Tc^{m}-HIDA is taken up by hepatocytes, probably by receptor mediated endocytosis (31). ^{99}Tc^{m}-HIDA is secreted into bile in its native state. Several studies have been reported on the use of ^{99}Tc^{m}-HIDA scintigraphy for the evaluation of liver function (32-36). Quantitative analysis (QA) of time-activity curves of the blood (blood retention ratio, plasma clearance) and liver (C_{max}, t_{max}, hepatic clearance index, $t_{½}$ uptake, $t_{½}$ excretion, mean transit time, hepatic excretion fraction) gives some indication of liver function.

The use of ^{99}Tc^{m}-HIDA scintigraphy in the detection of segmental bile duct obstruction due to tumour or intra-hepatic stones has been reported (37-40). ^{99}Tc^{m}- galactosyl-human serum albumin (GSA) is a new radiopharmaceutical for liver scintigraphy, selectively binding asialoglycoprotein receptors on the membranes of liver cells. The amount of ^{99}Tc^{m}-GSA accumulating in the liver has been found to correlate with severity in various liver diseases (41-44).

Most ^{99}Tc^{m}-HIDA studies involve planar (i.e. two-dimensional) registrations. In dynamic studies, regions of interest (ROI's) are placed in specific regions for the creation of time-activity curves. This technique, however, is strongly hampered in that it allows only gross assessment. Specific structures and diseased regions are difficult to localise and seldom possible to clearly project at planar registration. Furthermore, differences in volumes of liver tissue included in ROI's and inevitable inclusion of extra-hepatic tissue may influence findings.

Single photon emission computed tomography (SPECT) offers considerable increase in resolution. The three-dimensional evaluation allows greater precision in ROI placement without inclusion of unwanted over- or underlying tissue. Standardised thickness of reconstructed sections makes ROI's comparable, not only in terms of surface, but also in terms of volume and we suggest the future use of the term volume of interest (VOI) in this setting.

1.5 PRIMARY SCLEROSING CHOLANGITIS

Primary sclerosing cholangitis (PSC) is a chronic progressive cholestatic disease of unknown aetiology, characterised by progressive obliterating fibrosis of the intra- and extra-hepatic bile ducts (45, 46). It affects predominantly young men. An association with inflammatory bowel disease (IBD), usually ulcerative colitis, has been reported (47-50). The median survival from time of diagnosis is 9 to 12 years and in untreated patients will lead to premature death in 30-40 % (51-53). Five to twenty percent of patients can be expected to develop cholangiocarcinoma in the course of the disease (54-57). There is currently no generally accepted effective medical treatment for PSC. Several randomised controlled trials have shown that treatment with ursodeoxycholic acid (UDCA) improved serum liver function tests, but could not prove an effect on disease progression or survival (58-60). A recent study suggested that high dose UDCA (20 mg/kg/day) has a positive effect on histological stage, cholangiographic appearance and projected survival (61). The only definitive treatment is liver transplantation. There are, however, many controversies regarding patient selection for and timing of transplantation (51, 62).

Many attempts have been made to predict the notoriously unpredictable clinical course of patients with PSC. The Child-Pugh classification, initially developed as a tool to estimate hepatic functional reserve in candidates for porto-systemic shunt surgery, has been used (16, 63, 64). This classification focuses on patients with advanced cirrhotic changes, complicated by portal hypertension, and therefore lacks stratification and sensitivity in early liver disease. Several studies have assessed various demographic, clinical, biochemical and histological parameters as predictors of survival in PSC. Age, presence of IBD, clinical jaundice, ascites, history of variceal bleeding, hepatomegaly, splenomegaly, serum values of bilirubin, ALP, aspartate aminotransferase (AST), albumin, hemoglobin value and histological stage have been found to be independent predictors of survival. In attempts to make this information clinically applicable, several prognostic index formulas were developed (45, 54, 65-67). None of these formulas has been evaluated prospectively.

The currently most widely used prognostic scoring system is the revised Mayo natural history model as published by Kim et al, using serum levels of bilirubin, albumin, AST, a history of variceal bleeding and age as prognostic parameters (67). The risk score for a patient is calculated by adding the individual parameters, multiplied by their respective regression coefficients, quantifying the effects of variables on the risk of death. Survival can be estimated up to 4 years. Four of the parameters used in the scoring system are liver-related. Bilirubin generally represents the severity of cholestasis and albumin is an indicator of hepatic synthetic function. AST reflects ongoing hepatocyte destruction and can be used as an indicator of parenchymal inflammation. Variceal bleeding is a relatively coarse parameter, occurring in patients with advanced parenchymal disease. Age probably accounts for the general age-related mortality.

Endoscopic retrograde cholangio-pancreatography (ERCP) was the accepted golden standard for diagnosing PSC (68, 69). Several recent studies have shown good correlation between ERCP and magnetic resonance cholangio-pancreatography (MRCP) (70-72). MRCP, being less invasive and not being dependent on the presence of trans-papilliary administered contrast for visualisation of bile ducts, has replaced ERCP as cholangiographic method of choice for diagnosis. A number of studies have been reported on the value of ERCP as a

measure of disease severity and prognostic indicator for PSC (73-76). Results are contradicting, probably due to limitations of ERCP, but also to the lack of a standardised, functional classification system for cholangiographic findings in PSC. Different combinations of qualitative, quantitative and anatomical criteria have been used in efforts to create classification or grading systems, but none of these are generally accepted (68, 73, 74, 76, 77). MacCarty's classification is purely anatomical, not qualifying changes in the bile ducts (68). The classification used by Craig et al grades bile duct strictures according to three independent characteristics, evaluating intra- and extra-hepatic ducts separately (76). Van Laethem modified MacCarthy's classification by adding bile duct dilatation as qualitative parameter (73). Rajaram evaluates intra- and extra-hepatic ducts separately and grades changes qualitatively (77). Stockbrügger uses a qualitative scale for intra-hepatic ducts and a quantitative scale, based on percentage narrowing for the extra-hepatic ducts, including non-visualisation of peripheral intra-hepatic ducts as a criterium for the most advanced form of intra-hepatic disease (74). With the exception of Stockbrügger, non-visualisation, probably representing the most advanced form of intrahepatic disease, is not included in any of the classification systems.

A number of studies, the majority retrospective and none randomised, have shown clinical and biochemical improvement after treatment of radiologically detected dominant strictures by dilatation, stent placement or combination treatment (78-83). These results should be interpreted with extreme caution in a disease that is characterized by spontaneous episodic exacerbation and improvement. Criteria used to select and define a dominant stricture vary considerably between studies and bile duct dilatation proximal to strictures was often used as a criterion for significance. In patients with severe disease significant strictures are not necessarily associated with proximal dilatation. Increasing disease severity in PSC is associated with increasing fibrosis of ducts impeding the ability of ducts to dilate in response to flow obstruction. This could have led to a bias in patient selection, reserving therapy for the less severely affected group. Bear in mind that *dominance* does not imply *significance*! Unlike vascular surgery where methods exist to estimate the functional importance of radiologically detected lesions in vessels, no such methods exist for bile duct strictures.

The use of *planar* $^{99}Tc^{m}$-HIDA scintigraphy has been reported as a diagnostic modality in PSC. Brown et al used hepatic extraction fraction and excretion $t_{½}$ to differentiate between common bile duct obstruction, PSC and primary hepatocellular diseases as causes of jaundice (36). Rodman et al evaluated regional liver parenchymal function by drawing three ROI's according to a non-segmental template in the left and right liver (84). Significantly longer hepatic clearance excretion $t_{½}$ was found in PSC patients compared to normal volunteers. In some individual patients large variations in clearance half times from the three regions were recorded, consistent with regional differences in disease severity.

2 AIMS

The aims of this study were:

1. The creation of a dynamic liver function test, using tomographic imaging as sampling method, able to assess function on a segmental level;

2. Development of the technique for scintigraphy by using $^{99}Tc^{m}$-HIDA as test substance and SPECT as sampling method;

3. Application of the model in a normal volunteer population and patients with PSC;

4. Studying and mapping differences in left- and right-sided distribution of various radiopharmaceuticals in clinical use.

3 MATERIALS AND METHODS

3.1 PAPER I

Study population
Five patients with PSC and a control group of 5 healthy adult volunteers were included in the study. In patients the initial diagnosis was made on ERCP and confirmed on liver biopsy. All had CT or MR examinations of the liver performed at some stage during the course of the disease. Standard biochemical liver function tests and MRCP were performed at the time of scintigraphy.

Scintigraphy procedure
After an 8 hours fast, scintigraphy was performed using 120 MBq of $^{99}Tc^{m}$-HIDA (HIDASOL, Amersham Sorin S.r.l, Saluggia, Italy) injected in an anterior cubital vein. Acquisition of images started at the moment of radiopharmaceutical injection using a triple head gamma camera (Triad XLT, Trionix Inc., Twinsburg, OH, USA) equipped with low-energy ultra high-resolution parallel hole collimators and working on a 128x128 matrix. Twelve consecutive SPECT examinations, one every six minutes, were performed with the subject in supine. The camera heads were rotated in 45 steps in 360° with an acquisition time of 5 seconds per angle. Data were corrected on line with regard to energy, linearity and uniformity. The projections were pre-filtered with a 2D Hamming filter (cut-off frequency 1.40 cycles/cm) and sections were reconstructed using a ramp filter and filtered backprojection. Transverse tomographic sections with a nominal thickness of ~3 mm were reconstructed without correction for attenuation or scattering of photons. Spatial resolution of the camera is about 10 mm.

Evaluation
In patients, segmental landmarks were identified on the transaxial MR or CT sections and superimposed on SPECT sections. For the purpose of defining the segmental borders in the normal volunteers, the position of segmental boundaries was measured on CT scans of 20 patients with a normal finding at CT-examination and ranges and means were applied. ROI's were drawn on selected slices in segments II-VIII, avoiding the peripheries and central duct-rich areas and run on the same slices in all 12 studies. Segment I deviates anatomically from the segmental concept concerning blood supply and venous and biliary drainage and was excluded from analysis. Average counts per pixel were calculated and values were corrected for radioisotope decay. By plotting average counts per pixel of a ROI against the studies as performed at 6-minute intervals, a time-activity curve for each segment-representing ROI was created. QA for each curve was performed, measuring peak counts (C_{max}) and time point at peak counts (t_{max}) and calculating time after which counts decreased to 50 % of C_{max} (excretion $t_{½}$) using non-linear regression and one phase exponential decay. ERCP and MRCP (maximum intensity projection) images were visually evaluated and the status of segmental, sectorial, left and right main hepatic, common hepatic and common bile ducts described as normal, stenosed (stating the percentage if possible), dilated, beaded or not visualised. Liver biopsies were histologically staged according to Ludwig's classification (85). The QA of the scintigraphic data of patients was compared to that of the normal volunteers. In patients, QA was also correlated with cholangiographic findings, biochemical liver function tests and histological stage.

3.2 PAPER II

A virtual three-dimensional (3-D) model of a wedge-shaped bi-segmental liver sector was created using the computer aided design/computer aided manufacturing software Pro/ENGINEER, Release 20 (Parametric Technology Corporation, Upplands-Väsby, Sweden) running on a Silicon Graphics Octane Workstation (Silicon Graphics, Mountain View, CA, USA) (Figure 3).

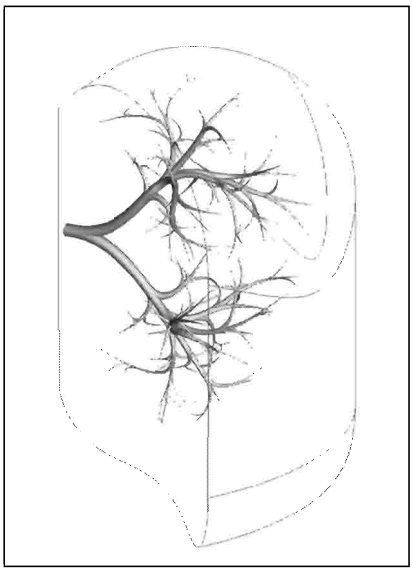

Figure 3. *The 3-D liver sector consisting of parenchyma and a system of bile ducts confluencing to form two segmental ducts and a sectorial duct*

Simulating the parenchyma and bile time-concentration curves of an ideal intravenously administered test substance with exclusive hepatic elimination and bile excretion and unidirectional inter-compartment flow, densities were awarded to the parenchymal mass and bile ducts in 12 identical sets of the model. The density values (mg/mm^3) approximated the activity (average counts/pixel) in the scintigraphic time-activity curves of the respective structures generated by dynamic $^{99}Tc^{m}$-HIDA scintigraphy in normal volunteers (**Paper 1**).

The virtual liver was sliced into 3 mm thick slices, similar to transversely reconstructed CT, MR or SPECT images. The resolution of the model enabled accurate placement of sampling ROI's in the parenchyma and specific bile ducts. By running the same ROI on the same slice on all 12 images, a dynamic time-density curve could be created for the ROI-represented structure. To solve the problem of detecting bile ducts in a low-resolution image, cranio-caudal density scanning (CCDS) was applied. The process involves the application of a semi-circular set of adjacent ROI's on each slice of the liver, starting with the most cranial through to the most caudal. By plotting the density in a ROI against the position (slice) in the liver, a 3-D density-position graph can be created for the specific set of ROI's, clearly showing areas with differences in density.

CCDS was performed on the model by creating three semi-circular sets of ROI's at different distances from the apex (Zones 1-3). Each ROI had a sampling volume of 20,2 mm^3. A 3-D density-position graph was created for each zone in all 12 liver sets. By applying the generating ROI of a specific density area on all 12 liver sets, a time-density curve, representative of that specific area could be created.

QA, including peak density (D_{max}), time point at peak density (Dt_{max}) and time after which the density decreased to 50 % of D_{max} (excretion $Dt_{½}$) was performed on the original, as well as ROI-created parenchymal and ductal time-density curves.

3.3 PAPER III

Twenty healthy adult volunteers, five males and fifteen females, age 22 to 57 years (mean 37), without history of liver disease were included in the study.

Scintigraphy procedure.
The scintigraphic procedure applied is identical to the protocol followed in **Paper I**.

Anatomical considerations
The mean values of the position of the segmental landmarks and the position of the portal vein bifurcation as measured on 50 CT examinations of patients with normal livers were used as the segmental borders in the subjects.

Cranio-caudal activity scanning (CCAS)
The confluence of the left and right hepatic ducts, situated at a point immediately anterior to the division of the main portal vein, was marked on the SPECT slice representing the transverse inter-segmental plane. With this point as the centre, a voxel-sized VOI was run in a 360° circular tract in every section cranial to caudal, recording counts per voxel. The procedure was performed with radii 5, 10, 15 and 20 voxels in all 12 SPECT acquisitions (Figure 4).

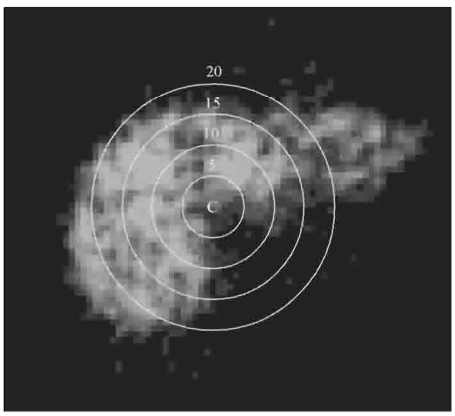

Figure 4. *A transverse reconstructed SPECT slice with the different sampling radii centred on the confluence of the right and left hepatic ducts (C)*

The data were acquired by a program written in C, running on a Unix workstation and imported into Excel 97 (Microsoft) by an application written in Visual Basic for Excel. Counts at every sampling point were plotted against x/y position and slice number, creating a position/activity graph for each sampling radius in each study, in total 48 graphs. Activity was colour-coded to show differences clearly and graphs could be manipulated three-dimensionally. Peaks, corresponding to ducts, could be seen clearly when isotope-rich bile started concentrating in the ducts, typically from SPECT 2 or 3 onwards. Extra-hepatic activity, for example gallbladder and stomach/duodenum, could be distinguished from hepatic activity. Sampling was done from segmental bile ducts, parenchyma, gallbladder and stomach/duodenum by selecting the relevant area of the spreadsheet data on any of the SPECT acquisitions, creating an annotated time-activity graph for the specific area. With the

position of segmental landmarks known, sampling could be done from parenchyma and ducts in the different segments (II-VIII). Segment I deviates anatomically from the segmental concept concerning blood supply and venous and biliary drainage and was excluded from analysis. For ducts the maximum activity in the sampling area was used, whereas the means of the counts in the VOI were calculated for the parenchymal, gallbladder and gastro-duodenal curves.

Quantitative and statistical analysis

QA for parenchymal and ductal curves was performed, measuring C_{max}, t_{max} and calculating excretion $t_{½}$ using non-linear regression and one phase exponential decay. Initial values were automatically calculated and the plateau constant fixed at zero. C_{max} and excretion $t_{½}$ values are given as means ± SD and t_{max} as medians. The Wilcoxon matched pairs test was used for comparing the results of QA from the left and right hemi-livers.

In one individual with QA results differing dramatically from the rest of the group, an MRCP was performed to exclude pathology.

3.4 PAPER IV

Twenty patients with PSC (10 male, 10 female), median age 43 (range 22-74), were included in the study. Initial diagnosis was made on findings at ERCP (n=15) or MRCP (n=5), and compatible clinical, biochemical and histologic findings. Patients with a long history and only an initial ERCP had an MRCP performed at the time of inclusion in the study, so that all subjects had a cholangiography performed within 14 months from scintigraphy. Standard biochemical liver function tests were performed at inclusion into the study. All subjects had standard CT or MR examinations of the liver performed within 14 months from scintigraphy.

Clinical evaluation
Clinical records were reviewed and the course of disease determined and classified as asymptomatic or symptomatic. The Mayo risk score for each patient was calculated using the revised natural history model for PSC (67). The Child-Pugh score was calculated using the modification as proposed by Pugh et al (16).

Scintigraphy procedure
The scintigraphic procedure applied is identical to the protocol followed in **Paper I**.

Cranio-caudal activity scanning
The positions of the segmental landmarks as seen on CT or MR examinations were measured for each individual patient. The position of the confluence of the left and right hepatic ducts, situated at a point immediately anterior to the division of the main portal vein, was also identified. The position of the hepatic confluence as measured on the CT/MR examinations was marked on the SPECT slice corresponding to the horizontal inter-segmental plane. Using this point as the centre, a voxel-sized VOI was run in a 360° circular tract in every section cranial to caudal, recording counts per voxel with radii 5, 10, 15 and 20 voxels in all 12 SPECT acquisitions. The data were acquired by a program written in C, running on a Unix workstation and imported into Excel 97 (Microsoft) by an application written in Visual Basic for Excel. Colour-coded position/activity graphs were created for each sampling radius in each study by plotting counts at every sampling point against x/y position and slice number. Segmental landmarks as determined on the CT/MR images were transposed onto these graphs, enabling localising of activity to specific segments. Duct-representing peaks were clearly visible. Sampling was done from segmental bile ducts and parenchyma, creating time-activity graphs of parenchyma and ducts for segments II to VIII. Segment I deviates anatomically from the segmental concept concerning blood supply and venous and biliary drainage and was excluded from analysis. For ducts, the maximum activity in the sampling area was used, whereas the mean of the counts in the VOI was calculated for the parenchyma. QA of curves was performed, measuring C_{max} and t_{max} and calculating excretion $t_{½}$ using non-linear regression and one phase exponential decay.

Cholangiographic evaluation
Cholangiographic images were evaluated separately by two consultant radiologists, unaware of clinical and scintigraphic findings, and reported as consensus. We created a cholangiography-based biliary classification to quantify the status of the bile flow path for each segment, based on the following assumptions:

- increasing stricturing implies increasing obstruction and decreasing flow, localised strictures ≥50 % being regarded as significant,
- dilated bile ducts are relatively normal and point to down-stream disease,
- beading is due to multiple strictures in a segment but can be the sick-duct response to a downstream obstruction,
- non-visualisation of ducts represents obliteration, the most advanced form of duct pathology.

The biliary tree was divided into extra-hepatic, left and right hepatic ducts, 4 sectorial ducts and 7 segmental ducts. Each duct was described as normal, dilated, strictured, beaded or not visualised. Strictures were defined as isolated when 1 cm or shorter (specifying < or ≥ 50 %) or diffuse when longer than 1 cm. Changes were quantified according to a scoring system as shown in Table 1. The values for the sectorial, hepatic, and extra-hepatic ducts for a specific sector were added to obtain a biliary score as quantitative assessment of the total bile-flow path for the sector.

Correlation of parameters

Cholangiographic biliary scores for sectorial, left and right hepatic and extra-hepatic ducts separately, as well as the added values for the bile-flow path of each sector, were correlated to the QA parameters of relevant segments. Mayo scores for the symptomatic and asymptomatic groups were compared. For each individual the mean C_{max} and excretion $t_{½}$ and median t_{max} values for ducts and parenchyma for the 7 segments were calculated as a total liver QA and correlated with the calculated Mayo risk score as well as the individual biochemical parameters included in the score.

Table 1. *Scoring system for bile duct changes as observed on cholangiography*

Score	Cholangiographic parameter
0	Normal, dilated or isolated stricture <50 %
1	Isolated stricture ≥50 % or diffuse stricture
2	Beading
3	Non-visualisation

Statistical analysis

The Spearman rank order correlation test was used for correlation of scintigraphic data with the cholangiographic biliary scores, Mayo score and individual biochemical parameters. A p-value <0.05 was considered statistically significant.

3.5 PAPER V

Patients
Patients were examined with either [^{123}I]- metaiodobenzylguanidine (MIBG) (n=19), ^{111}In-pentetreotide (n=26) or ^{99}Tc^{m}-labelled monoclonal antibody against granulocytes (MoAb) (n=18). Indications for [^{123}I]-MIBG scintigraphy were suspected phaeochromocytoma or paraganglioma and for ^{111}In-pentetreotide scintigraphy were suspected carcinoid tumour, insulinoma or gastrinoma. The indication for examination with ^{99}Tc^{m}-labelled MoAb was a suspected focal non-chronic bacterial infection. Inclusion criteria were: 1) no known history of or risk factor for liver disease; 2) an even activity distribution in the liver without focal lesions, except for a difference between the two hemi-livers; 3) a left hemi-liver considered to be sufficiently bulky to allow a representative evaluation; 4) chemical liver test made within ±3 months from the examination showing ALP within the normal range and at least one other liver test within the normal range. In all three radiopharmaceutical groups there were a number of examinations showing pathological uptake *outside* the liver.

Healthy volunteers
Twenty normal subjects were examined with ^{99}Tc^{m}-HIDA SPECT.

Radiopharmaceuticals
Subjects received 148 MBq of [^{123}I]-MIBG, Mallinckrodt Medical B.V., Petten, The Netherlands), 122 MBq of ^{111}In-pentetreotide ([^{111}In-DTPA-D-Phe^{1}]-octreotide, OctreoScan®, Mallinckrodt Medical B.V.), 500 MBq of ^{99}Tc^{m}-labelled MoAb (Anti-Granulocyte BW 250/183, CIS MEDIPRO SA, Vernier Genève, Switzerland) or 120 MBq of ^{99}Tc^{m}-HIDA (HIDASOL, Amersham Sorin S.r.l., Saluggia, Italy) intravenously. The radiopharmaceutical purity of each batch of the ^{99}Tc^{m}-labelled MoAb and ^{99}Tc^{m}-HIDA labelling kits was routinely tested with regard to free pertechnetate by thin-layer chromatography.

SPECT examination
SPECT registrations were performed 20-24 hours after intravenous administration of [^{123}I]-MIBG and ^{111}In-pentetreotide and after 3-5 hours (early) and 20-24 hours (late) for ^{99}Tc^{m}-labelled MoAb. Patients examined with ^{111}In-pentetreotide were prepared by laxatives and enemas. All examinations were performed on the same dual head gamma camera (Biad XLT, Trionix Inc., Twinsburg, OH, USA) equipped with high-resolution low-energy parallel hole collimators (^{99}Tc^{m} and ^{123}I) or middle-energy parallel hole collimators (^{111}In). SPECT was carried out in 120 steps in 360^{o} with a total examination time of 40 min. The matrix size was 128x128. Energy windows of 20 % were centered around the 159 keV peak for ^{123}I, the 140 keV peak for ^{99}Tc^{m}, and the 171 and 245 keV peaks for ^{111}In. Acquisition data were corrected with regard to energy, linearity and uniformity. The projections were prefiltered with a 2D Hamming filter, and reconstructed with a ramp filter and filtered backprojection. Correction was made for attenuation but not for scattering of photons. In the ^{99}Tc^{m}-HIDA group, the scintigraphic procedure applied was identical to the protocol followed in Paper I. Only the first (1-4 minutes) and the second (7-10 minutes) acquisitions were evaluated. Correction was made for attenuation but not for scattering of photons.

Evaluation

All studies were evaluated by adding 2-4 consecutive reconstructed transverse sections through the cranial liver portion. ROI's were drawn in the central portions of the left and right hemi-livers that are divided by vertical plane represented by the course of the middle hepatic vein (Cantlie's line). Edges, indentations and the gall bladder fossa were avoided. In a few cases, a second set of sections at a different level had to be assessed in order to evaluate representative portions of both hemi-livers. The background activity was assessed by a large ROI in the lower abdomen. Activity from the urinary tracts, adrenals, large bowel and any pathological uptake was avoided. After correcting for the number of sections and for ROI size, the activity concentration ratios between the left and right hemi-livers and between the hemi-livers and the background activity were calculated.

Statistics

The one sample t-test was used for the statistical evaluation. Values are given as mean ± SD.

Ethical considerations (I, III – V)

Informed consent was obtained from all subjects prior to examinations and the studies were approved by the local ethics and radiation safety committees.

4 RESULTS

4.1 PAPER I

QA of the normal volunteers is shown in Table 2. Cholangiographic findings and QA results for the patients are summarised in Table 3.

Table 2. *QA of normal volunteers. The values at the bottom of the table are for all segments*

	C_{max}	t_{max}	$t_{½}$
Segment	Mean ± SD	Mean ± SD	Mean ± SD
II	20.7 ± 11.1	18 ± 5.0	17.8 ± 6.40
III	17.0 ± 10.6	18 ± 5.0	20.7 ± 6.40
IV	26.7 ± 6.6	18 ± 5.0	20.9 ± 5.36
V	35.3 ± 10.1	18 ± 5.0	21.5 ± 2.35
VI	27.1 ± 10.8	18 ± 5.0	20.2 ± 2.93
VII	27.1 ± 9.9	18 ± 5.0	18.2 ± 1.82
VIII	32.3 ± 11.3	18 ± 5.0	19.6 ± 3.95
Total	26.6 ± 11.0	18 ± 4.6	19.8 ± 4.3

All patients had intra-hepatic disease, while in two the extra-hepatic ducts were normal. One patient (Patient 4, Table 3) had segmental intra-hepatic disease, with the right hemi-liver radiologically unaffected. This was evident on the time-activity curves with more horizontal excretion curves of the left-sided segments compared to the right, resulting in relatively longer excretion $t_{½}$ values of segments II, III and IV compared to segments V, VI, VII and VIII (Figure 5).

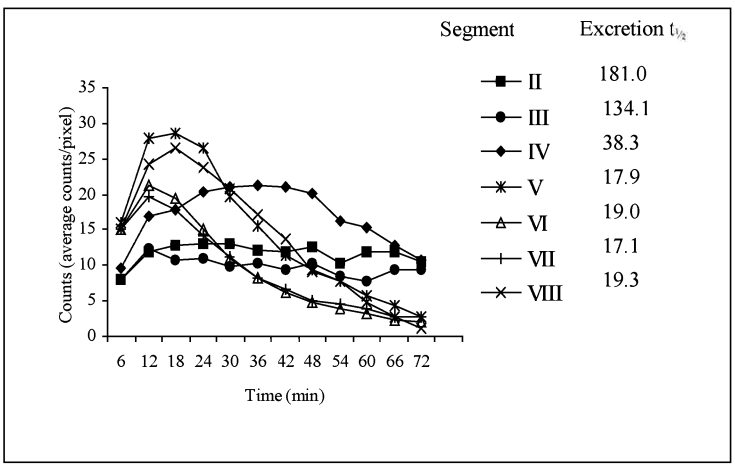

Figure 5. *Time-activity curves of the patient with segmental intra-hepatic disease*

The time-activity curves of patients with diffuse intra-hepatic disease showed delayed excretion from all segments, reflected in excretion $t_{½}$ values considerably longer than those of the normal volunteers. The longest excretion $t_{½}$ values were recorded in the patient who had clinically and radiologically the most severe disease. In some of the individual patients large inter-segmental variations in t_{max} values were noted. A trend of longer excretion $t_{½}$ and lower C_{max} values in patients with more severely disturbed liver function tests was observed. Patients with histologically stage IV disease had longer excretion $t_{½}$ and lower C_{max} values than patients with Stage II and III disease.

Table 3. *Patients: QA compared to ERCP/MRCP findings. Bile ducts were graded as N (normal); S (stenosed, stating percentage if possible); D (dilated); B (beaded); X (not visualised). (CHD – common hepatic duct) (CBD – common bile duct)*

Segment	QA			Cholangiographic findings				
	C_{max}	t_{max}	$t_{½}$	Segment	Sector	Main hepatic	CHD	CBD
Patient 1								
II	8.7	18	64.6	X	B	B	X	N
III	7.1	12	459.7	X				
IV	8.9	42	48.0	X	B			
V	11.4	12	141.7	X	B	B		
VIII	11.6	18	131.4	X				
VI	11.3	42	81.4	X	X			
VII	10.3	24	113.9	X				
Patient 2								
II	17.5	12	146.8	X	B	D	N	N
III	23.1	18	126.0	X				
IV	14.7	18	196.4	X	X			
V	26.1	24	109.8	X	B	N		
VIII	19.4	18	135.4	X				
VI	8.0	12	67.2	X	X			
VII	25.0	24	87.4	X				
Patient 3								
II	13.9	12	105.8	N	D	B	D	N
III	9.6	24	123.8	X				
IV	16.9	18	76.8	D	B			
V	19.6	18	84.2	S	B	B		
VIII	18.8	18	61.2	S				
VI	13.6	36	95.3	S	B			
VII	14.8	12	113.1	S				
Patient 4								
II	13.1	24	181.0	X	D	D	S(50)	N
III	12.2	12	134.1	D				
IV	21.2	36	38.3	X	X			
V	28.6	18	17.9	N	N	D		
VIII	26.5	18	19.0	N				
VI	21.2	12	17.1	N	N			
VII	19.6	12	19.3	N				
Patient 5								
II	33.0	18	40.5	X	B	S(50)	N	N
III	28.1	18	36.9	X				
IV	49.1	18	55.0	X	X			
V	49.6	18	30.2	B	B	S(50)		
VIII	48.7	18	46.6	B				
VI	35.0	18	29.4	X	B			
VII	34.6	18	49.1	X				

4.2 PAPER II

The 3 mm transverse slices of the high-resolution liver demonstrated the good definition of structures (Figure 6a). Sampling ROI's could be placed accurately and ROI recreated time-density curves representing the parenchyma and bile ducts were identical to the original curves.

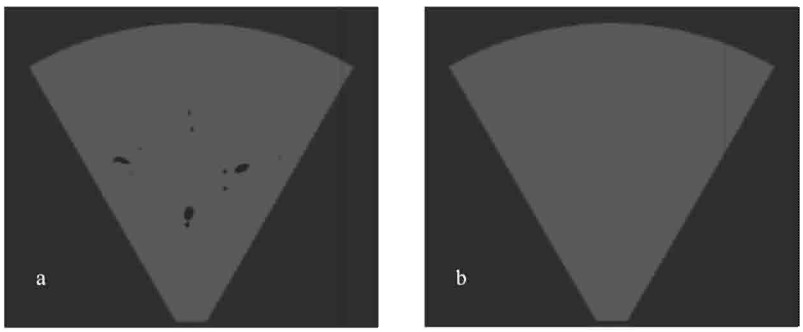

Figure 6. *Example of a transverse slice of (a) the high-resolution and (b) the low-resolution model. The good definition of structures in the high-resolution image enabled accurate ROI placement in parenchyma and different bile ducts. On the low-resolution image individual structures are not visible*

On the slices of the low-resolution model, the ducts were indistinguishable from the surrounding parenchyma (Figure 6b). Performing CCDS on these slices revealed three distinct curve types when plotting density against the position in the liver (Figure 7).

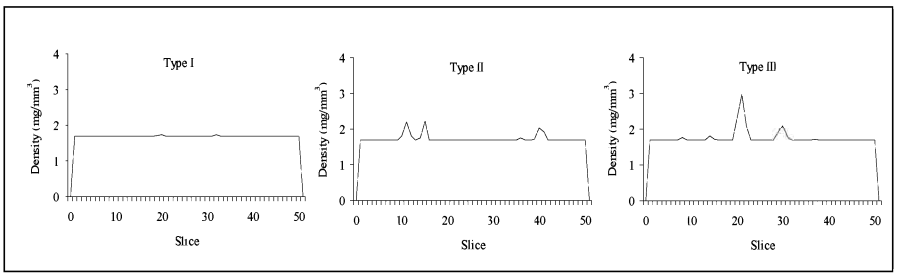

Figure 7. *Types of density-position curves as seen on CCDS of the liver model. Peaks corresponded to the presence of ducts in the ROI's, the height being proportional to the percentage of the sampling volume occupied by duct*

Type I curves rose to a plateau as the ROI started cutting liver tissue and maintained an even plateau until exit. Type II curves rose to a plateau with multiple small spiked peaks superimposed on the plateau. In Type III curves a spiked plateau with one or two high peaks was observed. In the first three image sets, where parenchymal and ductal densities were more or less equal, all ROI's in all three zones created Type I curves. In the last 9 image sets, where differences between the densities occurred, Zone I ROI's still created only Type I curves, as the volume of the ducts included in the sampling volumes were too small to influence the total

sampling volume density significantly. Zone II ROI's, however, created Type I and II curves and Zone III Type I, II and III. In Figure 8 the Zone I, II and III 3-D density graphs for image set 4 are shown. The graphs mirrored the zonal cut planes in the model, with the peaks corresponding to ducts and the plateau to parenchyma. The height of a peak was proportional to the percentage of the sampling volume occupied by duct. In the highest Zone II peak 69.7 % of the total sampling volume consisted of duct and in the highest Zone III peak 98.3%.

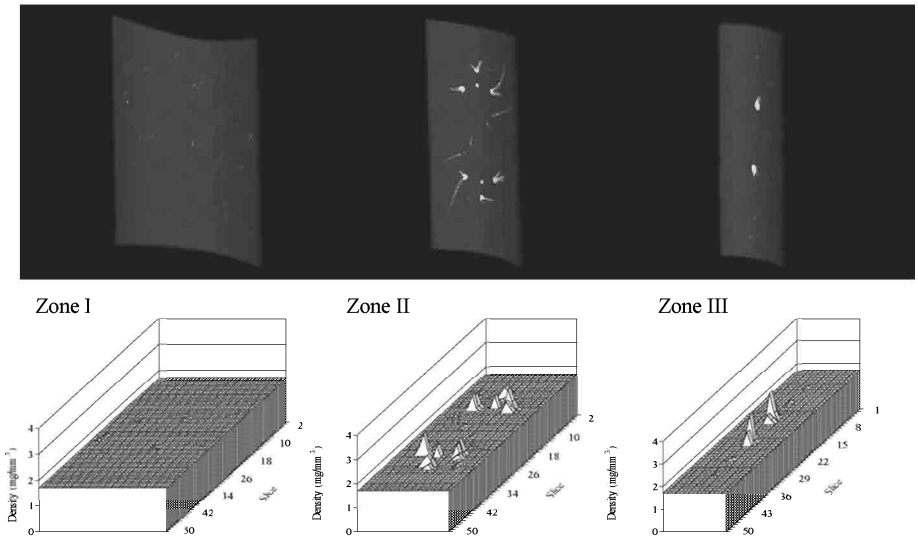

Figure 8. *Zone I, II and III 3-D density graphs for image set 4. The graphs mirror the zonal cut planes in the model, with the plateau corresponding to parenchyma and the peaks to ducts*

Time-density curves were created for one of the plateau-generating ROI's in Zone I and the ROI's generating the highest peaks in Zones II and III (Figure 9). The ROI from Zone I generated a time-density curve that matched the original parenchymal curve and the Zone III ROI a curve almost identical to the original ductal curve. The Zone II curve fell between the two original curves.

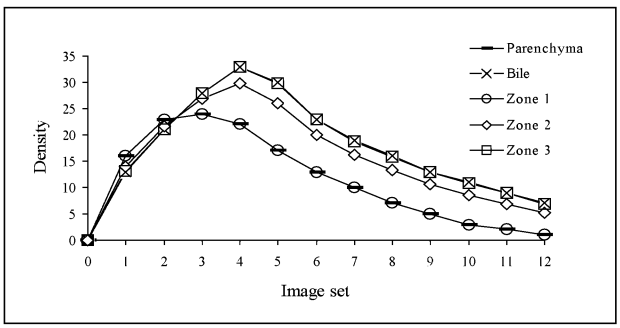

Figure 9. *Time-density curves for a plateau-generating ROI from Zone I and the ROI's generating the highest peaks in Zone II and III. Zone I and III curves match the original parenchymal and ductal curves respectively*

The results of QA of the original and ROI-generated curves are shown in Table 4. The D_{max}, Dt_{max} and excretion $Dt_{½}$ of the Zone I curve were identical to the parenchymal values and the Zone III results closely matched those of the original ductal curve. QA of the Zone II curves produced results falling between those of the original curves.

Table 4. *QA of the original and ROI-generated curves*

	D_{max} (mg/mm^3)	D_{tmax} (minutes)	$D_{t½}$ (minutes)
Parenchyma	2.40	15.0	13.5
Duct	3.30	20.0	18.2
Zone I	2.40	15.0	13.5
Zone II	2.97	20.0	16.5
Zone III	3.28	20.0	18.1

4.3 PAPER III

In Figure 10 activity graphs of SPECT acquisitions 1, 4 and 12 of one representative subject are shown. Ductal peaks were best visible on the fourth acquisition. Distinctly different patterns of duct-representing peaks were observed for each sampling radius. Central sampling resulted in graphs with relatively few but high-pitched peaks. Increasing the sampling radius resulted in more numerous but smaller peaks. This relates to activity in different generation bile ducts, detected at different radii. The right and left hepatic ducts could usually be seen on the 5 voxel graphs, sectorial ducts on the 10 and 15 voxel graphs and segmental ducts on the 15 and 20 voxel graphs. At least one segmental duct could be identified for each segment in all subjects. Gallbladder and intestinal (gastro-duodenal) activity can clearly be seen on acquisition 12.

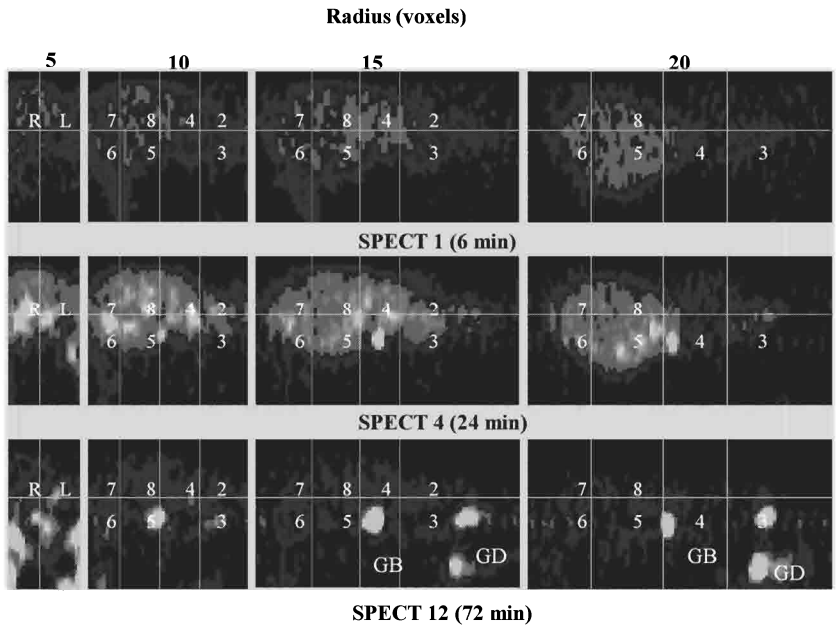

Figure 10. *Activity/position graphs for sampling radii 5, 10, 15 and 20 of SPECT studies 1, 4 and 12. Segmental landmarks are drawn in and segments numbered. Note the presence of ductal peaks on SPECT 4 and gallbladder (GB) and gastro-duodenal (GD) activity on SPECT 12*

Distinctly different time/activity curves were found for the various structures (Figure 11). Parenchymal and ductal curves were of the typical uptake-excretion type. Gallbladder curves showed a consistent and steep increase in activity as isotope-rich bile was concentrated in the gallbladder reaching a plateau towards the end of the study. Gastric and duodenal curves were typically ragged as bile secreted into the duodenum and refluxed into the stomach, was cleared by peristalsis.

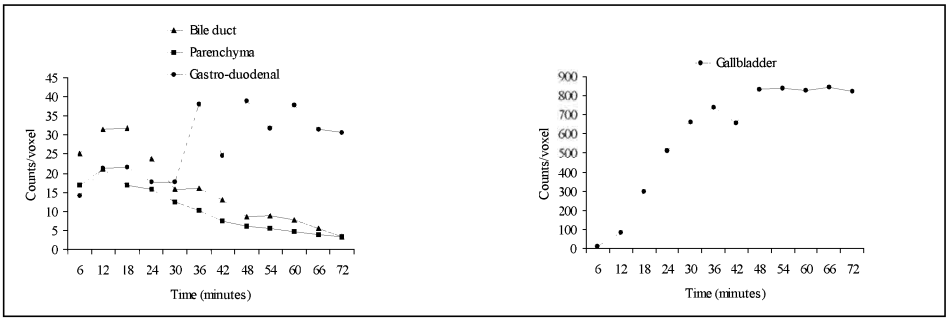

Figure 11. *Parenchymal, ductal, gallbladder and gastro-duodenal time/activity curves of a subject*

Parenchyma

C_{max} of left-sided segments (24.7±8.9) was significantly lower than the values for right-sided segments (33.2±10.4) ($p<0.001$). This was a consistent finding (100 % of subjects). Excretion $t_{½}$ of the left-sided segments (26.9±6.3) was significantly longer than the values on the right side (24.0±5.7) ($p=0.002$), an occurrence in 75 % of individuals. No difference in the t_{max} between left and right-sided segments was found.

Ducts

There was no difference in C_{max} for ducts draining left and right-sided segments. Excretion $t_{½}$ and t_{max} were, however, significantly longer for ducts draining left-sided segments ($p=0.023$ and $p<0.001$ respectively). Longer excretion $t_{½}$ and longer t_{max} for the left-sided ducts were present in 15 (75 %) and 16 (80 %) of subjects respectively. In one subject the difference was alarmingly large and an MRCP was performed to exclude liver pathology. It was normal but showed drainage of the right posterior sector (segments 6 and 7) into the left hepatic duct.

4.4 PAPER IV

The demographic and clinical parameters of subjects are summarised in Table 5.

Table 5. *Demographic and clinical characteristics of patients*

Variable	Median (range) or n (proportion (%))
Age (years)	43 (22-74)
Gender (male)	10 (50 %)
Duration of disease (months)	97 (1-258)
Associated IBD	15 (75 %)
Ulcerative colitis	13 (65 %)
Crohns disease	2 (10 %)
History: variceal bleeding	0 (0 %)
Current course	
Asymptomatic	7 (35 %)
Symptomatic	13 (65 %)

Mayo risk scores for the total group ranged from -0.84 to 3.22 (mean 0.29). For the asymptomatic and symptomatic groups the mean Mayo risk scores were -0.21 (-0.84 to 0.74) and 0.57 (-0.78 to 3.22), respectively.

In certain patients, large variations in uptake and clearance from different segments were noted, indicating non-homogenous disease. Duct-representing peaks could be identified in all segments in 18 patients (90 %). In two patients clear duct activity could not be distinguished from parenchymal activity. They had Mayo scores of 3.22 and 1.27 respectively. The first had a projected four-year survival of 18 % and died 2 months after scintigraphy. The second patient had a projected four-year survival of 79 % and subsequently underwent liver transplantation.

Cholangiographic correlation
Cholangiographic findings indicated diffuse intra-hepatic disease in all patients. In four patients the extra-hepatic ducts were assessed as normal.

There was a statistically significant correlation between the segmental biliary and parenchymal excretion $t_{½}$ and biliary scores for the sectorial, the left and right hepatic ducts and added biliary score (Table 6). However, on a sectorial and left and right hepatic level a supposedly significant stricture was in some, but not all accompanied by decreased bile flow. This probably indicates that some of these lesions lacked functional importance.

Table 6. *Correlation between segmental QA parameters and biliary score in different generations ducts and added biliary score*

	Duct $t_{½}$	Parenchyma $t_{½}$
	r_s (p-value)	
Sectorial	0.25 (0.004)	0.19 (0.02)
Left and right hepatic	0.23 (0.01)	0.22 (0.009)
Extra-hepatic	-0.07 (0.44)	-0.04 (0.65)
Added biliary score	0.21 (0.002)	0.23 (0.006)

Mayo score and biochemical correlation

The parenchymal and ductal excretion $t_{½}$ and t_{max} values showed a statistically significant positive correlation with the Mayo risk score. A negative correlation was observed between C_{max} for both parenchyma and ducts but only the parenchymal correlation reached statistical significance (Table 7). Total bilirubin, being an indicator of cholestasis, had a positive correlation with excretion $t_{½}$ for both parenchyma and duct but only the parenchymal correlation reached statistical significance. A statistically significant negative correlation between bilirubin and parenchymal C_{max} and positive correlation with parenchymal t_{max} were shown. AST, being an indicator of hepato-cellular destruction, showed a negative correlation with parenchymal C_{max} and ductal C_{max}. Albumin showed a positive statistically significant correlation with parenchymal excretion $t_{½}$.

Table 7. *Correlation between Mayo risk score and QA parameters*

Parameter		r_s	p-value
Duct	C_{max}	-0.36	0.13
	$t_{½}$	0.50	0.04
	t_{max}	0.59	0.007
Parenchyma	C_{max}	-0.61	0.004
	$t_{½}$	0.49	0.03
	t_{max}	0.51	0.03

4.5 PAPER V

Liver activity versus background activity
The liver could be distinguished in all examinations. In the [^{123}I]-MIBG subjects, the mean ±SD activity ratio between the left hemi-liver and background activity was 3.47±0.96, and between the right hemi-liver and background 2.78±0.62. Corresponding ratios for of ^{99}Tc^{m}-labelled MoAb early were 12.8±11.7 and 13.0±12.2, for of ^{99}Tc^{m}-labelled MoAb late 7.41±7.66 and 7.52±7.74, for ^{111}In-pentetreotide 6.33±3.06 and 7.05±3.42, for ^{99}Tc^{m}-HIDA first 6.36±4.34 and 9.42±6.16 and for ^{99}Tc^{m}-HIDA second 14.1±10.6 and 20.8±13.3 respectively.

Ratios between the hemi-livers
From the examinations with [^{123}I]-MIBG, a mean activity concentration ratio between the left and right hemi-liver >1 was calculated. The examinations with ^{111}In-pentetreotide and ^{99}Tc^{m}-HIDA gave a ratio <1. The examinations with ^{99}Tc^{m}-labelled MoAb showed no difference between the hemi-livers (Table 8).

Table 8. *Left/right hemi-liver activity ratio for the different radiopharmaceuticals*

		Activity ratio - left/right (mean ±SD)	p-value[#]
[^{123}I]-MIBG		1.25±0.21	p<0.001
^{111}In-pentetreotide		0.90±0.09	p<0.001
^{99}Tc^{m}-labelled MoAb	early (3-5 h)	0.98±0.06	p=0.32
	late (20-24 h)	0.99±0.11	p=0.75
^{99}Tc^{m}-HIDA	first	0.68±0.12	p<0.001
	second	0.66±0.12	p<0.001

[#]Null hypothesis: The mean ratio in the population = 1.

Changes over time
There was no statistically significant difference of the activity ratios between early and late of ^{99}Tc^{m}-labelled MoAb (p=0.83) or between first and second ^{99}Tc^{m}-HIDA (p=0.47).

5 DISCUSSION

The number of different liver function tests in clinical use and that are being experimented with in the literature, is an indication that none of the current available tests are optimal. The ultimate liver function test is probably QA of a dynamic test. The test substance for such a test should be safe, well tolerated, without interaction with concomitant medications and not influenced by diet, nutritional status or genetic factors. The kinetics of the substance should be well characterised, simple and suitable from a time perspective. Excretion should be exclusively by the liver and it should preferably have unidirectional inter-compartment flow. Currently used dynamic tests use serum sampling, limiting sampling from a single input compartment. Furthermore, the creation of dynamic studies suitable for QA requires repetitive sampling, making serum sampling unpractical and expensive. Imaging-based sampling solves these problems. It is non-invasive, making it practical for repetitive sampling. Access for measuring the test substance in the organs involved in the kinetics of the substance is only limited by the resolution of the imaging procedure.

An imaged-based liver function test, as demonstrated in the computerised simulation, can be applied with any tomographic imaging technique for which a suitable test substrate exists, including SPECT, CT and MR. The availability of suitable test substances in the form of the $^{99}Tc^{m}$-HIDA analogues makes SPECT an attractive option as sampling device. One disadvantage, however, is poor resolution making the identification of different structures, especially intra-hepatic, difficult. We have solved the problem by applying CCAS and creating software to make the procedure quick and user-friendly. The resolution achieved by CT and MR is much better. Unfortunately, suitable test substances for CT or MR are not currently available. Meglumine compounds used for biliary enhancement during CT have a biliary excretion of 75-90 %, but an unacceptable incidence of side effects (86-88). Hepatocyte-selective contrast agents are available for use in MR imaging. Mangafodipir (Mn-DPDP) has a plasma half-life of 120 minutes. Gadolinium ethoxybenzyl diethylenetriaminepentaacetic acid (Gd-EOB-DTPA) has more favourable pharmacokinetic qualities with a plasma half-life of 10 minutes. Unfortunately, hepatic excretion of both substances is low, 47 % and 50 % respectively, making them unsuitable for use in a dynamic test (89, 90).

An imaging-based dynamic test, using an intravenously administered test substance excreted into bile, would allow sampling from four different compartments (blood-pool, hepatic parenchyma, bile ducts and gut). One could even subdivide the bile duct compartment into sub-compartments for different generation bile ducts. Dynamic time-activity curves, suitable for QA, can be created for each compartment and sub-compartment. This would allow evaluation of plasma clearance, hepatocyte uptake and excretion and flow of the test substance in different generation bile ducts. Apart from an assessment of total liver function, the functional integrity of parenchyma and bile ducts can be evaluated separately on a segmental level. Such a test has several potential clinical applications.

Some diseases, including PSC, primary intra-hepatic stones and Caroli's disease, affect the liver non-homogeneously. They are primarily cholangiopathies with secondary parenchymal changes depending on the extent of the ductal disease. Currently used liver function tests, evaluating the liver as a whole, lack sensitivity in these diseases. Due to the large reserve capacity of the liver, conventional liver function tests can be normal or only marginally

disturbed in patients with advanced segmental pathology. A comprehensive imaging-based liver function test, enabling differentiation between ductal and parenchymal contributions to deranged liver function may have particular application in these diseases.

We chose PSC as clinical model for testing the method and showing its potential advantages for a variety of reasons:

1. It is a non-homogeneous liver disease, primarily a cholangiopathy with secondary parenchymal involvement.
2. Both ductal and parenchymal pathology contribute to liver dysfunction.
3. Prediction of prognosis in PSC patients is notoriously difficult.
4. The optimal timing of treatment options is controversial and evaluation of treatment outcome, for example after stricture dilatation, is difficult.

In our study, results of the dynamic SPECT used as an indicator of total hepatic capacity correlated well with the revised Mayo risk score. The technique, as a measuring tool for total hepatic function can be improved. We have used the means and median of segmental values as an estimate of total liver function, resulting in segments contributing equally to the total value. It is, however, known from volumetric studies that significant differences and a large inter-individual range exist in volumes of the different segments (91). Adjusting the QA values from individual segments according to the percentage of the total liver volume represented by the specific segment will give a more accurate estimate of total liver function.

The non-existence of a method to measure segmental function and bile flow makes evaluation of the new method difficult. The cholangiographic biliary score was an effort to create some standard to compare with the segmental results of the dynamic test. Many points concerning our classification are debatable. As in previous quantitative classification systems, we have used percentage of narrowing for grading. The cut-off of 50 % was chosen in accordance with guidelines used in vascular surgery. Using the actual diameter of the stricture may be more appropriate and less prone to inter-observer variation. We have not used segmental cholangiographic findings in our correlation. MRCP, as currently used, has limited sensitivity in the evaluation of the segmental ducts. Non-visualisation could therefore be due to limitations of the method and does not necessarily imply advanced disease.

Our technique may aid in the management of patients with PSC. Although percutaneous liver biopsy is not mandatory for the diagnosis of PSC, it is frequently used for confirming the diagnosis. It has been shown to have independent prognostic value and is included in some of the prognostic scoring systems. Regional variations in disease activity may result in random biopsies not being taken from the worst affected parts, and the use of paired biopsies has been suggested (92). The QA findings can direct biopsies to the most affected parts of the liver, making them more representative. QA of bile duct curves may allow assessment of radiologically detected isolated strictures in terms of bile flow obstruction. Furthermore, the functional status of parenchyma drained by the diseased duct can be evaluated. This may aid in more judicious selection of strictures for therapy. The effect of therapy can be evaluated by comparing pre- and post-intervention studies. Rapidly deteriorating drainage of a specific segment on serial studies may alert one to the possibility of a cholangiocarcinoma as the cause of obstruction. Monitoring progression of both parenchymal damage and biliary obstruction by means of sequential studies could complement existing multivariate survival models in the prediction of outcome and selection and timing of therapeutic procedures.

Post-operative hepatic failure is the leading cause of hospital mortality following resectional liver surgery (93). Cultural beliefs in the Orient and shortage of donors in the West have prompted the development of living-donor liver transplants (94-97). Ensuring sufficient liver tissue to sustain life for both donor and recipient in living-donor liver transplants is critical. In an adult with normal hepatic parenchyma, up to 70 % of total liver volume can be resected (98, 99). A number of methods have been used to establish hepatic functional reserve and to predict post-operative functional status. Standard serum liver function tests have not been shown to have any predictive value (100). Dynamic testing with ICG has been found to be superior to amino acid and aminopyrine clearance for evaluating pre-operative functional reserve (93). Scintigraphic studies using $^{99}Tc^{m}$-GSA for determining asialoglycoprotein receptor concentration have been found to be of value (101, 102). Liver volume calculations, mainly using CT volumetric analysis have been used (91, 103, 104). Volume measurements are based on the assumption that regional liver function is uniform throughout the liver. In cirrhosis, function per unit hepatic volume is not uniform throughout the liver (105). Our findings, suggesting that functional capacity is non-homogeneous in normal livers, are supported by a study using $^{99}Tc^{m}$-GSA (106). Expressing total liver function as the total of the product of volume and segmental function in individual segments, may give a more accurate estimate of total liver function. Combining a dynamic test, able to analyse both parenchymal and duct function with a volumetric method may prove to be superior to previously used methods and be of help in safer decision-making.

Regional functional differences

The purpose of the study in normal volunteers was to determine normal values for the quantitative parameters of the test and to document possible differences between different liver segments. We describe, as far as we know for the first time, quantitative differences in biliary kinetics between the left and right hemi-livers. The results of our study with [^{123}I]-MIBG, ^{111}In-pentetreotide and $^{99}Tc^{m}$-labelled MoAb support the theory of non-vascular physiological differences between the hemi-livers. Physiological differences between the left and right hemi-livers may play a role in the non-homogeneity of some liver diseases. It may furthermore explain well known but so far undocumented observations made at cholangiography.

Differences between the development of the left and the right hemi-livers are present from early embryological growth. The developing left hemi-liver receives exclusively placental blood, whereas the right hemi-liver is perfused by placental blood and blood from the foetal portal system. Portal venous blood contains hepatotrophic substances from pancreatic origin (insulin and glucagon) as well as HGF, produced in the spleen (4-6, 107). During foetal life only the right hemi-liver is exposed to these substances on first pass. This may result in differences between the development of left- and right-sided hepatocytes.

Even in post-foetal life, differences exist in blood flow between the right and left hemi-livers. Portal flow is considered to be laminar, resulting in incomplete mixing of the blood after entering the portal vein from the respective feeding veins. Preferential distribution of blood flowing from the superior mesenteric vein and splenic vein into the right portal and left portal veins was first suggested in the early 1900's (108, 109). These findings have been confirmed using modern techniques, including portal venography, scintigraphy and MR angiography (110-112). The effect of this preferential supply is unequal exposure of the left and right

hemi-livers to hepatotrophic factors from the spleen and pancreas even in adult life, the bulk of these substances going through the left hemi-liver on first pass.

The streamlining of portal blood may explain the preferential hemi-liver distribution shown by some diseases. It may be the mechanism of the tendency of right-sided colon cancers to metastasise to the right hemi-liver (113). The right hemi-liver predominance of some infectious diseases may also depend on this mechanism. Approximately 75 % of hepatic hydatid cysts occur in the right hemi-liver (114). Pyogenic and amoebic liver abscesses also show right hemi-liver predominance (115-118). Atrophy of the right hemi-liver and hypertrophy of the left in patients with alcoholic cirrhosis are well documented (119-121). Absorption of ingested alcohol is into the superior mesenteric vein, exposing the right hemi-liver to higher concentrations of alcohol on first pass (122). Furthermore, blood from the splenic vein, supplying the left hemi-liver, is more oxygenated, which, with uneven portal distribution of hepatotrophic growth factors generated outside the liver, may explain the slower progression of cirrhosis in the left hemi-liver (123). In a series of patients with lobar atrophy without cirrhosis or tumour, atrophy of the right hemi-liver was always associated with marked reactive enlargement of the left hemi-liver, but atrophy of the left hemi-liver did not induce the same degree of enlargement in the right (124).

Williams et al have commented on left hepatic duct predominance on $^{99}Tc^{m}$-HIDA scintigraphy (125). They mention the drainage of one of the sectorial ducts from the right hemi-liver into the left hepatic duct, occurring in 17-34 % of individuals as a probable cause (126). Our study in normal volunteers showed slower bile flow in left-sided bile ducts compared to the right in 75 % of subjects. In the normal subject with the largest difference in left and right-sided excretion $t_{½}$, MRCP showed drainage of the right posterior sector into the left hepatic duct. Biliary flow differences may explain the uneven distribution of primary intra-hepatic stones. Intra-hepatic stone formation secondary to trans-papillary biliary invasion of Clonorchis sinensis (Chinese liver fluke) and Ascaris lumbricoides is endemic in East Asian countries (127, 128). Even outside the Orient, reports suggested an association with Ascariasis (129, 130). These stones occur in the left-sided intra-hepatic ducts in the majority of cases (131-133). The slower bile flow in the left-sided intra-hepatic biliary ducts may be the reason why parasites prefer this location for settling after having fought an upstream battle against the might of common bile duct flow. Endoscopists are familiar with the fact that bile duct dilatation secondary to obstruction in the choleduchus occurs earlier and is more marked in the left hemi-liver in spite of the fact that approximately two thirds of hepatocyte volume usually drain into the right-sided ducts. This occurrence may be the result of flow differences.

Uneven distribution of copper and iron between the hemi-livers of new-borns has been reported (134, 135). In Wilson's disease higher copper concentrations were observed in the right hemi-liver (136).

6 CONCLUSIONS

The idea of a dynamic liver function test, using tomographic imaging as sampling method, as demonstrated in the computer model, seems feasible. It enables assessment of different aspects of hepatic function for the total liver, as well as in individual segments. Although $^{99}Tc^{m}$-HIDA approximates the perfect test substance in terms of its pharmaco-kinetic characterisitics, SPECT poses some problems as imaging sampling method. Its poor spatial resolution made identification of intrahepatic ducts difficult. This was solved by the creation of software simplifying the application of CCAS for detection of intra-hepatic ducts.

Through application of dynamic $^{99}Tc^{m}$-HIDA SPECT in a normal volunteer population, normal values for the different QA parameters could be established. Furthermore, results showed clear differences in biliary kinetics between the left and right hemi-livers that we could quantify.

In patients with PSC results of dynamic $^{99}Tc^{m}$-HIDA SPECT correlated with currently used indicators of disease severity and on a segmental level correlated with cholangiographic findings. We are confident that the method may be of value in the management of PSC patients, both as a prognostic indicator and as an aid in clinical decision-making. In particular, the ability to quantify bile duct strictures in terms of bile flow obstruction may have important clinical application. Selection of strictures for intervention can be based on the actual effect of the stricture in terms of flow obstruction. Furthermore, pre- and post-intervention studies will give objective evidence of the result of intervention.

The results of our study with [^{123}I]-MIBG, ^{111}In-pentetreotide and $^{99}Tc^{m}$-labelled MoAb lend further support to the theory that the liver is not a uniform organ, and that non-vascular physiological differences exist between the two hemi-livers. These differences may play a role in the pathogenesis of liver diseases with hemi-liver preferences. Such differences are also important to keep in mind when interpreting scintigraphic studies.

Extending the principle to other tomographic imaging procedures as CT and MR, is a simple conceptual step. Hopefully development of suitable hepato-specific contrast agents with suitable kinetic characteristics will make this a reality in the not too distant future.

Financial support

The author acknowledges with great appreciation financial support from:
The Swedish Research Council
Bengt Ihre Foundation
Ruth and Rickard Juhlin Foundation
Karolinska Institutet

7 ACKNOWLEDGEMENTS

I wish to express my sincere gratitude to all who have contributed to realising this work. My special thanks to:

Corinne, Julia and Claudia for their never-ending love and support, in spite of my all too often absence of mind.

My father and late mother, Piet and Denise Jonas, for their unfailing love and support, and teaching me the importance of perseverance.

Rolf Hultcrantz, my supervisor and tutor, for his support and critical reflections on my ideas, channelling them into the clinical field.

Hans Jacobsson, my co-supervisor and tutor in nuclear medicine, for his contagious enthusiasm, patient help, and for being a constant source of bright ideas.

Erik Näslund, my co-supervisor and colleague, for sharing his wisdom on science and bureaucracy and support on all levels.

Premysl Slezak, my dear friend and tutor, for being the driving force behind the initiation of this project and for his continuous support.

Nicklas Miller for his skillful creation of the liver model.

My co-authors, PO Schnell, Lennart Blomqvist and Anna-Carin Sjösteen for their respective contributions that made this work possible.

Stig Larsson and the fantastic personnel in the Department of Nuclear Medicine, Karolinska Hospital, for always being willing to help, finding time for examinations and letting me borrow their expensive machines.

Colleagues in the Department of Gastroenterology and Hepatology, Karolinska Hospital, where I paced the first steps on this journey, in particular Ragnar Befrits and Per Hellström.

Lars Granström, head of Upper GI surgery, Danderyd Hospital for creating an excellent work environment and Zeunerts®.

My colleagues and fellow 2002 graduates (beating me at it) in the Upper GI section. Jacob Freedman, for helping with al the byte problems. Dag Stockeld for sharing his reflections on life.

Lars Backman, previous head of Upper GI surgery and my first contact at Danderyd Hospital, whose shoes I try to fill in vain.

Per-Anders Flordal and Staffan Gröndal, previous and current heads of the Department of Surgery, Danderyd Hospital, for allowing me to work where I am.

My colleagues in the Department of Surgery, the staff in the wards and endoscopy unit, and secretaries (that have to create sense out of my particular version of the Swedish language) for making it a pleasure to work there.

All patients and volunteers, without whom this work would not have been possible.

8 REFERENCES

1. Kroeber AL. Anthropology. London: George G. Harrap; 1948.
2. Bartholin T. Vasa lymphatica nuper hafniae in animalibus inventa et hepatis exsequiae. Copenhagen: Hafniae; 1653.
3. Arey L. A Textbook and Laboratory Manual of Embryology. Philadelphia: W.B. Saunders; 1965.
4. Court FG, Wemyss-Holden SA, Dennison AR, Maddern GJ. The mystery of liver regeneration. Br J Surg 2002;89(9):1089-95.
5. Matsumoto K, Nakamura T. Roles of HGF as a pleiotropic factor in organ regeneration. Exs 1993;65:225-49.
6. Starzl TE, Francavilla A, Halgrimson CG, Francavilla FR, Porter KA, Brown TH, et al. The origin, hormonal nature, and action of hepatotrophic substances in portal venous blood. Surg Gynecol Obstet 1973;137(2):179-99.
7. Bismuth H. Surgical anatomy and anatomical surgery of the liver. World J Surg 1982;6(1):3-9.
8. Cantlie J. On a new arrangement of the left and right lobes of the liver. Proc Anat Soc Great Britain Ireland 1897;32:4-9.
9. Healey J, Schroy P. Anatomy of the biliary ducts within the human liver; analysis of the prevailing pattern of branchings and the major variations of the biliary ducts. Arch Surg 1953;66:599-616.
10. Hjortsjö C. The topography of the intrahepatic duct systems. Acta Anat 1951;11:599-615.
11. McIndoe A, Counseller V. The bilaterality of the liver. Arch Surg 1927;15:589-612.
12. Bismuth H, Houssin D, Castaing D. Major and minor segmentectomies "reglees" in liver surgery. World J Surg 1982;6(1):10-24.
13. Couinaud C. Le Foie. Etudes anatomiques et chirurgicales. Paris: Masson; 1957.
14. Strasberg SM. Terminology of liver anatomy and liver resections: coming to grips with hepatic Babel. J Am Coll Surg 1997;184(4):413-34.
15. Brockmöller J, Roots I. Assessment of liver metabolic function. Clinical implications. Clin Pharmacokinet 1994;27(3):216-48.
16. Pugh RN, Murray-Lyon IM, Dawson JL, Pietroni MC, Williams R. Transection of the oesophagus for bleeding oesophageal varices. Br J Surg 1973;60(8):646-9.
17. Frederiks WM, Myagkaya GL, Bosch KS, Fronik GM, van Veen H, Vogels IM, et al. The value of enzyme leakage for the prediction of necrosis in liver ischemia. Histochemistry 1983;78(4):459-72.
18. Rosalki SB, Foo AY, Dooley JS. Benign familial hyperphosphatasaemia as a cause of unexplained increase in plasma alkaline phosphatase activity. J Clin Pathol 1993;46(8):738-41.
19. Reichen J. MEGX test in hepatology: the long-sought ultimate quantitative liver function test? J Hepatol 1993;19(1):4-7.
20. Figg WD, Dukes GE, Lesesne HR, Carson SW, Songer SS, Pritchard JF, et al. Comparison of quantitative methods to assess hepatic function: Pugh's classification, indocyanine green, antipyrine, and dextromethorphan. Pharmacotherapy 1995;15(6):693-700.
21. Freys G, Pottecher T, Calon B, Hamel G, Pain L, Boudjema K, et al. Early assessment of transplanted liver function: lignocaine clearance test (MEGX). Eur J Anaesthesiol 1997;14(4):397-405.
22. Shinohara H, Tanaka A, Kitai T, Yanabu N, Inomoto T, Satoh S, et al. Direct measurement of hepatic indocyanine green clearance with near- infrared spectroscopy: separate evaluation of uptake and removal. Hepatology 1996;23(1):137-44.

23. Jalan R, Hayes PC. Review article: quantitative tests of liver function. Aliment Pharmacol Ther 1995;9(3):263-70.
24. Delprat G, Epstein N, Kerr W. A new liver function test : the elimenation of rose bengal when injected into the circulation of human subjects. Arch Intern Med 1924;34:533-541.
25. Cohn E, Zagerman J, Sklaroff D, Tumen H. The use of radioactive rose bengal as a test in the differential diagnosis of jaundice. Am J Gastroenterol 1957;28:621-628.
26. Eyler WR, Schuman BM, Du Sault LA, Hinson RA. Rose bengal I-131 liver scan. An aid in the differential diagnosis of jaundice. Jama 1965;194(9):990-2.
27. Nordyke RA. Metabolic and physiologic aspects of 131 I rose bengal in studying liver function. Semin Nucl Med 1972;2(2):157-66.
28. Winston MA, Blahd WH. 131 I rose bengal imaging techniques in differential diagnosis of jaundiced patients. Semin Nucl Med 1972;2(2):167-75.
29. Loberg MD, Cooper M, Harvey E, Callery P, Faith W. Development of new radiopharmaceuticals based on N-substitution of iminodiacetic acid. J Nucl Med 1976;17(7):633-8.
30. Krishnamurthy S, Krishnamurthy GT. Technetium-99m-iminodiacetic acid organic anions: review of biokinetics and clinical application in hepatology. Hepatology 1989;9(1):139-53.
31. Okuda H, Nunes R, Vallabhajosula S, Strashun A, Goldsmith SJ, Berk PD. Studies of the hepatocellular uptake of the hepatobiliary scintiscanning agent 99mTc-DISIDA. J Hepatol 1986;3(2):251-9.
32. Ekman M, Fjalling M, Friman S, Carlson S, Volkmann R. Liver uptake function measured by IODIDA clearance rate in liver transplant patients and healthy volunteers. Nucl Med Commun 1996;17(3):235-42.
33. Hawkins RA, Hall T, Gambhir SS, Busuttil RW, Huang SC, Glickman S, et al. Radionuclide evaluation of liver transplants. Semin Nucl Med 1988;18(3):199-212.
34. McGinty MP, Stewart RM, Fabian MJ, Fabian TC, Proctor KG. Gamma-scintigraphy and early hepatocellular dysfunction during posttraumatic sepsis. Surgery 1994;116(3):535-43.
35. Tagge EP, Campbell DA, Jr., Reichle R, Averill DR, Jr., Merion RM, Dafoe DC, et al. Quantitative scintigraphy with deconvolutional analysis for the dynamic measurement of hepatic function. J Surg Res 1987;42(6):605-12.
36. Brown PH, Juni JE, Lieberman DA, Krishnamurthy GT. Hepatocyte versus biliary disease: a distinction by deconvolutional analysis of technetium-99m IDA time-activity curves. J Nucl Med 1988;29(5):623-30.
37. Zeman RK, Gold JA, Gluck L, Caride VJ, Burrell M, Hoffer PB. Tc-99m HIDA scintigraphy in segmental biliary obstruction. J Nucl Med 1981;22(5):456-8.
38. Yeh SH, Liu RS, Chiu PF, Wu LC, Liu OK, Huang MJ. Technetium-99m HIDA hepatic lobar distribution and retention ratios in detection of intrahepatic lithiasis. J Nucl Med 1985;26(3):241-9.
39. Gupta S, Owshalimpur D, Cohen G, Margules R, Herrera N. Scintigraphic detection of segmental bile-duct obstruction. J Nucl Med 1982;23(10):890-1.
40. Aburano T, Taniguchi M, Hisada K, Miyazaki Y, Kakuma K, Fujioka M. Discordant hepatic uptake of Tc-99m HIDA and Tc-99m colloid in a patient with segmental biliary obstruction. Clin Nucl Med 1988;13(8):599-601.
41. Kudo M, Todo A, Ikekubo K, Hino M, Yonekura Y, Yamamoto K, et al. Functional hepatic imaging with receptor-binding radiopharmaceutical: clinical potential as a measure of functioning hepatocyte mass. Gastroenterol Jpn 1991;26(6):734-41.
42. Ha-Kawa SK, Nakanishi Y, Kojima M, Tanaka Y, Kitagawa S, Kubota Y, et al. [Clinical application of asialoglycoprotein receptor-mediated liver scintigraphy using

99mTc-DTPA-galactosyl-human serum albumin]. Nippon Igaku Hoshasen Gakkai Zasshi 1991;51(12):1489-97.
43. Koizumi K, Uchiyama G, Arai T, Ainoda T, Yoda Y. A new liver functional study using Tc-99m DTPA-galactosyl human serum albumin: evaluation of the validity of several functional parameters. Ann Nucl Med 1992;6(2):83-7.
44. Torizuka K, Ha-Kawa SK, Kudo M, Kubota Y, Yamamoto K, Itoh K, et al. [Phase III multi-center clinical study on 99mTc-GSA, a new agent for functional imaging of the liver]. Kaku Igaku 1992;29(2):159-81.
45. Wiesner RH, Grambsch PM, Dickson ER, Ludwig J, MacCarty RL, Hunter EB, et al. Primary sclerosing cholangitis: natural history, prognostic factors and survival analysis. Hepatology 1989;10(4):430-6.
46. Ueno Y, LaRusso NF. Primary sclerosing cholangitis. J Gastroenterol 1994;29(4):531-43.
47. Sivak MV, Jr., Farmer RG, Lalli AF. Sclerosing cholangitis: its increasing frequency of recognition and association with inflammatory bowel disease. J Clin Gastroenterol 1981;3(3):261-6.
48. Rabinovitz M, Gavaler JS, Schade RR, Dindzans VJ, Chien MC, Van Thiel DH. Does primary sclerosing cholangitis occurring in association with inflammatory bowel disease differ from that occurring in the absence of inflammatory bowel disease? A study of sixty-six subjects. Hepatology 1990;11(1):7-11.
49. Cangemi JR, Wiesner RH, Beaver SJ, Ludwig J, MacCarty RL, Dozois RR, et al. Effect of proctocolectomy for chronic ulcerative colitis on the natural history of primary sclerosing cholangitis. Gastroenterology 1989;96(3):790-4.
50. Fausa O, Schrumpf E, Elgjo K. Relationship of inflammatory bowel disease and primary sclerosing cholangitis. Semin Liver Dis 1991;11(1):31-9.
51. Eckhauser FE, Colleti LM, Knol JA. The changing role of surgery for sclerosing cholangitis. Dig Dis 1996;14(3):180-91.
52. Harnois DM, Lindor KD. Primary sclerosing cholangitis: evolving concepts in diagnosis and treatment. Dig Dis 1997;15(1-2):23-41.
53. Olsson R, Danielsson Å, Järnerot G, Lindström E, Lööf L, Rolny P, et al. Prevalence of primary sclerosing cholangitis in patients with ulcerative colitis. Gastroenterology 1991;100(5 Pt 1):1319-23.
54. Broomé U, Olsson R, Lööf L, Bodemar G, Hultcrantz R, Danielsson Å, et al. Natural history and prognostic factors in 305 Swedish patients with primary sclerosing cholangitis. Gut 1996;38(4):610-5.
55. Kornfeld D, Ekbom A, Ihre T. Survival and risk of cholangiocarcinoma in patients with primary sclerosing cholangitis. A population-based study. Scand J Gastroenterol 1997;32(10):1042-5.
56. Rosen CB, Nagorney DM, Wiesner RH, Coffey RJ, Jr., LaRusso NF. Cholangiocarcinoma complicating primary sclerosing cholangitis. Ann Surg 1991;213(1):21-5.
57. Chalasani N, Baluyut A, Ismail A, Zaman A, Sood G, Ghalib R, et al. Cholangiocarcinoma in patients with primary sclerosing cholangitis: a multicenter case-control study. Hepatology 2000;31(1):7-11.
58. Beuers U, Spengler U, Kruis W, Aydemir U, Wiebecke B, Heldwein W, et al. Ursodeoxycholic acid for treatment of primary sclerosing cholangitis: a placebo-controlled trial. Hepatology 1992;16(3):707-14.
59. Lindor KD. Ursodiol for primary sclerosing cholangitis. Mayo Primary Sclerosing Cholangitis-Ursodeoxycholic Acid Study Group. N Engl J Med 1997;336(10):691-5.
60. Stiehl A, Walker S, Stiehl L, Rudolph G, Hofmann WJ, Theilmann L. Effect of ursodeoxycholic acid on liver and bile duct disease in primary sclerosing cholangitis. A 3-year pilot study with a placebo- controlled study period. J Hepatol 1994;20(1):57-64.

61. Mitchell SA, Bansi DS, Hunt N, Von Bergmann K, Fleming KA, Chapman RW. A preliminary trial of high-dose ursodeoxycholic acid in primary sclerosing cholangitis. Gastroenterology 2001;121(4):900-7.
62. Ahrendt SA, Pitt HA, Kalloo AN, Venbrux AC, Klein AS, Herlong HF, et al. Primary sclerosing cholangitis: resect, dilate, or transplant? Ann Surg 1998;227(3):412-23.
63. Shetty K, Rybicki L, Carey WD. The Child-Pugh classification as a prognostic indicator for survival in primary sclerosing cholangitis. Hepatology 1997;25(5):1049-53.
64. Kim WR, Poterucha JJ, Wiesner RH, LaRusso NF, Lindor KD, Petz J, et al. The relative role of the Child-Pugh classification and the Mayo natural history model in the assessment of survival in patients with primary sclerosing cholangitis. Hepatology 1999;29(6):1643-8.
65. Farrant JM, Hayllar KM, Wilkinson ML, Karani J, Portmann BC, Westaby D, et al. Natural history and prognostic variables in primary sclerosing cholangitis. Gastroenterology 1991;100(6):1710-7.
66. Dickson ER, Murtaugh PA, Wiesner RH, Grambsch PM, Fleming TR, Ludwig J, et al. Primary sclerosing cholangitis: refinement and validation of survival models. Gastroenterology 1992;103(6):1893-901.
67. Kim WR, Therneau TM, Wiesner RH, Poterucha JJ, Benson JT, Malinchoc M, et al. A revised natural history model for primary sclerosing cholangitis. Mayo Clin Proc 2000;75(7):688-94.
68. MacCarty RL, LaRusso NF, Wiesner RH, Ludwig J. Primary sclerosing cholangitis: findings on cholangiography and pancreatography. Radiology 1983;149(1):39-44.
69. Ayoola EA, Vennes JA, Silvis SE, Rohrmann CA, Ansel HJ. Endoscopic retrograde intrahepatic cholangiography in liver diseases. Gastrointest Endosc 1976;22(3):156-9.
70. Ernst O, Asselah T, Sergent G, Calvo M, Talbodec N, Paris JC, et al. MR cholangiography in primary sclerosing cholangitis. AJR Am J Roentgenol 1998;171(4):1027-30.
71. Fulcher AS, Turner MA, Franklin KJ, Shiffman ML, Sterling RK, Luketic VA, et al. Primary sclerosing cholangitis: evaluation with MR cholangiography-a case-control study. Radiology 2000;215(1):71-80.
72. Vitellas KM, Enns RA, Keogan MT, Freed KS, Spritzer CE, Baillie J, et al. Comparison of MR cholangiopancreatographic techniques with contrast- enhanced cholangiography in the evaluation of sclerosing cholangitis. AJR Am J Roentgenol 2002;178(2):327-34.
73. Van Laethem JL, Devière J, Bourgeois N, Love J, Gelin M, Cremer M, et al. Cholangiographic findings in deteriorating primary sclerosing cholangitis. Endoscopy 1995;27(3):223-8.
74. Stockbrügger RW, Olsson R, Jaup B, Jensen J. Forty-six patients with primary sclerosing cholangitis: radiological bile duct changes in relationship to clinical course and concomitant inflammatory bowel disease. Hepatogastroenterology 1988;35(6):289-94.
75. Olsson RG, Asztely MS. Prognostic value of cholangiography in primary sclerosing cholangitis. Eur J Gastroenterol Hepatol 1995;7(3):251-4.
76. Craig DA, MacCarty RL, Wiesner RH, Grambsch PM, LaRusso NF. Primary sclerosing cholangitis: value of cholangiography in determining the prognosis. AJR Am J Roentgenol 1991;157(5):959-64.
77. Rajaram R, Ponsioen CY, Majoie CB, Reeders JW, Lameris JS. Evaluation of a modified cholangiographic classification system for primary sclerosing cholangitis. Abdom Imaging 2001;26(1):43-7.
78. Baluyut AR, Sherman S, Lehman GA, Hoen H, Chalasani N. Impact of endoscopic therapy on the survival of patients with primary sclerosing cholangitis. Gastrointest Endosc 2001;53(3):308-12.

79. Kaya M, Petersen BT, Angulo P, Baron TH, Andrews JC, Gostout CJ, et al. Balloon dilation compared to stenting of dominant strictures in primary sclerosing cholangitis. Am J Gastroenterol 2001;96(4):1059-66.
80. Linder S, Söderlund C. Endoscopic therapy in primary sclerosing cholangitis: outcome of treatment and risk of cancer. Hepatogastroenterology 2001;48(38):387-92.
81. Stiehl A, Rudolph G, Kloters-Plachky P, Sauer P, Walker S. Development of dominant bile duct stenoses in patients with primary sclerosing cholangitis treated with ursodeoxycholic acid: outcome after endoscopic treatment. J Hepatol 2002;36(2):151-6.
82. van Milligen de Wit AW, van Bracht J, Rauws EA, Jones EA, Tytgat GN, Huibregtse K. Endoscopic stent therapy for dominant extrahepatic bile duct strictures in primary sclerosing cholangitis. Gastrointest Endosc 1996;44(3):293-9.
83. Johnson GK, Geenen JE, Venu RP, Schmalz MJ, Hogan WJ. Endoscopic treatment of biliary tract strictures in sclerosing cholangitis: a larger series and recommendations for treatment. Gastrointest Endosc 1991;37(1):38-43.
84. Rodman CA, Keeffe EB, Lieberman DA, Krishnamurthy S, Krishnamurthy GT, Gilbert S, et al. Diagnosis of sclerosing cholangitis with technetium 99m-labeled iminodiacetic acid planar and single photon emission computed tomographic scintigraphy. Gastroenterology 1987;92(3):777-85.
85. Ludwig J. Surgical pathology of the syndrome of primary sclerosing cholangitis. Am J Surg Pathol 1989;13(Suppl 1):43-9.
86. Dohmen JP, Lemmens JA, Lamers JJ. A double-blind comparison of meglumine iotroxate (Biliscopin) and meglumine iodoxamate (Cholovue). Diagn Imaging 1981;50(6):305-8.
87. Cohen MD, Herman E, Herron D, White SJ, Smith JA. Comparison of intravenous contrast agents for CT studies in children. Acta Radiol 1992;33(6):592-5.
88. McClennan BL, Heiken JP, Lee JK, James MA. Computed body tomography with a new nonionic contrast agent. Comparison of ioversol with sodium/meglumine diatrizoate. Invest Radiol 1989;24 Suppl 1:S35-8.
89. Hahn PF, Saini S. Liver-specific MR imaging contrast agents. Radiol Clin North Am 1998;36(2):287-97.
90. Semelka RC, Helmberger TK. Contrast agents for MR imaging of the liver. Radiology 2001;218(1):27-38.
91. Leelaudomlipi S, Sugawara Y, Kaneko J, Matsui Y, Ohkubo T, Makuuchi M. Volumetric analysis of liver segments in 155 living donors. Liver Transpl 2002;8(7):612-4.
92. Olsson R, Hagerstrand I, Broomé U, Danielsson Å, Järnerot G, Lööf L, et al. Sampling variability of percutaneous liver biopsy in primary sclerosing cholangitis. J Clin Pathol 1995;48(10):933-5.
93. Lau H, Man K, Fan ST, Yu WC, Lo CM, Wong J. Evaluation of preoperative hepatic function in patients with hepatocellular carcinoma undergoing hepatectomy. Br J Surg 1997;84(9):1255-9.
94. Tanaka K, Kiuchi T. Living-donor liver transplantation in the new decade: perspective from the twentieth to the twenty-first century. J Hepatobiliary Pancreat Surg 2002;9(2):218-22.
95. Trotter JF, Wachs M, Everson GT, Kam I. Adult-to-adult transplantation of the right hepatic lobe from a living donor. N Engl J Med 2002;346(14):1074-82.
96. Lo CM, Fan ST, Liu CL, Wei WI, Lo RJ, Lai CL, et al. Adult-to-adult living donor liver transplantation using extended right lobe grafts. Ann Surg 1997;226(3):261-9; discussion 269-70.
97. Yamaoka Y, Washida M, Honda K, Tanaka K, Mori K, Shimahara Y, et al. Liver transplantation using a right lobe graft from a living related donor. Transplantation 1994;57(7):1127-30.

98. Pol B, Campan P, Hardwigsen J, Botti G, Pons J, Le Treut YP. Morbidity of major hepatic resections: a 100-case prospective study. Eur J Surg 1999;165(5):446-53.
99. Fan ST, Lo CM, Liu CL, Yong BH, Chan JK, Ng IO. Safety of donors in live donor liver transplantation using right lobe grafts. Arch Surg 2000;135(3):336-40.
100. Hemming AW, Scudamore CH, Shackleton CR, Pudek M, Erb SR. Indocyanine green clearance as a predictor of successful hepatic resection in cirrhotic patients. Am J Surg 1992;163(5):515-8.
101. Kokudo N, Vera DR, Tada K, Koizumi M, Seki M, Matsubara T, et al. Predictors of Successful Hepatic Resection: Prognostic Usefulness of Hepatic Asialoglycoprotein Receptor Analysis. World J Surg 2002;26(11):11.
102. Hwang EH, Taki J, Shuke N, Nakajima K, Kinuya S, Konishi S, et al. Preoperative assessment of residual hepatic functional reserve using 99mTc-DTPA-galactosyl-human serum albumin dynamic SPECT. J Nucl Med 1999;40(10):1644-51.
103. Tudoret L. [Measurement of the volume of the liver by 3D computed tomography with anatomic correlation]. Ann Radiol 1994;37(5):401-4.
104. Kamel IR, Kruskal JB, Warmbrand G, Goldberg SN, Pomfret EA, Raptopoulos V. Accuracy of volumetric measurements after virtual right hepatectomy in potential donors undergoing living adult liver transplantation. AJR Am J Roentgenol 2001;176(2):483-7.
105. Matsuzaki S, Onda M, Tajiri T, Kim DY. Hepatic lobar differences in progression of chronic liver disease: correlation of asialoglycoprotein scintigraphy and hepatic functional reserve. Hepatology 1997;25(4):828-32.
106. Imaeda T, Kanematsu M, Asada S, Seki M, Doi H, Saji S. Utility of Tc-99m GSA SPECT imaging in estimation of functional volume of liver segments in health and liver diseases. Clin Nucl Med 1995;20(4):322-8.
107. Ueki T, Kaneda Y, Tsutsui H, Nakanishi K, Sawa Y, Morishita R, et al. Hepatocyte growth factor gene therapy of liver cirrhosis in rats. Nat Med 1999;5(2):226-30.
108. Bartlett F, Corper H, Long E. The independance of the lobes of the liver. Am J Physiol 1914;35:36-50.
109. Serege H. Hepatic lobar distribution of portal circulation. J Med Bord 1901;31(271-314).
110. Moore G, Bridenbaugh R. Roentgen demonstration of the venous circulation in the liver: portal venography. Radiology 1951;57:685-90.
111. Kashiwagi T, Kimura K, Suematsu T, Schichiri M, Kamada T, Abe H. Heterogeneous intrahepatic distribution of blood flow in humans. Eur J Nucl Med 1981;6(12):545-9.
112. Gallix BP, Reinhold C, Dauzat M, Bret PM. Streamlined flow in the portal vein: demonstration with MR angiography. J Magn Reson Imaging 2002;15(5):603-9.
113. Shirai Y, Wakai T, Ohtani T, Sakai Y, Tsukada K, Hatakeyama K. Colorectal carcinoma metastases to the liver. Does primary tumor location affect its lobar distribution? Cancer 1996;77(11):2213-6.
114. Yorganci K, Sayek I. Surgical treatment of hydatid cysts of the liver in the era of percutaneous treatment. Am J Surg 2002;184(1):63-9.
115. Abuabara SF, Barrett JA, Hau T, Jonasson O. Amebic liver abscess. Arch Surg 1982;117(2):239-44.
116. Jamaiah I, Shekhar KC. Amoebiasis: a 10 year retrospective study at the University Hospital, Kuala Lumpur. Med J Malaysia 1999;54(3):296-302.
117. Cuaron A, Gordon F. Liver scanning: analysis of 2,500 cases of amebic hepatic abscesses. J Nucl Med 1970;11(7):435-9.
118. Chou FF, Sheen-Chen SM, Chen YS, Chen MC. Single and multiple pyogenic liver abscesses: clinical course, etiology, and results of treatment. World J Surg 1997;21(4):384-8; discussion 388-9.

119. Torres WE, Whitmire LF, Gedgaudas-McClees K, Bernardino ME. Computed tomography of hepatic morphologic changes in cirrhosis of the liver. J Comput Assist Tomogr 1986;10(1):47-50.
120. Shreiner DP, Barlai-Kovach M. Diagnosis of alcoholic cirrhosis with the right-to-left hepatic lobe ratio: concise communication. J Nucl Med 1981;22(2):116-20.
121. Harbin WP, Robert NJ, Ferrucci JT, Jr. Diagnosis of cirrhosis based on regional changes in hepatic morphology: a radiological and pathological analysis. Radiology 1980;135(2):273-83.
122. Garcia JE, Atkins F. A low right-to-left hepatic lobe ratio. Is streamlining of ethanol to the right lobe of the liver the cause? Clin Nucl Med 1985;10(11):807-9.
123. Ring JA, Ghabrial H, Ching MS, Shulkes A, Smallwood RA, Morgan DJ. Propranolol elimination by right and left fetal liver: studies in the intact isolated perfused fetal sheep liver. J Pharmacol Exp Ther 1998;284(2):535-41.
124. Ishida H, Naganuma H, Konno K, Komatsuda T, Hamashima Y, Ishioka T, et al. Lobar atrophy of the liver. Abdom Imaging 1998;23(2):150-3.
125. Williams W, Krishnamurthy GT, Brar HS, Bobba VR. Scintigraphic variations of normal biliary physiology. J Nucl Med 1984;25(2):160-5.
126. Kawarada Y, Das BC, Taoka H. Anatomy of the hepatic hilar area: the plate system. J Hepatobiliary Pancreat Surg 2000;7(6):580-6.
127. Chen HH, Zhang WH, Wang SS, Caruana JA. Twenty-two year experience with the diagnosis and treatment of intrahepatic calculi. Surg Gynecol Obstet 1984;159(6):519-24.
128. Pausawasdi A, Watanapa P. Hepatolithiasis: epidemiology and classification. Hepatogastroenterology 1997;44(14):314-6.
129. Schulman A. Non-western patterns of biliary stones and the role of ascariasis. Radiology 1987;162(2):425-30.
130. Schulman A. Intrahepatic biliary stones: imaging features and a possible relationship with ascaris lumbricoides. Clin Radiol 1993;47(5):325-32.
131. Chijiiwa K, Yamashita H, Yoshida J, Kuroki S, Tanaka M. Current management and long-term prognosis of hepatolithiasis. Arch Surg 1995;130(2):194-7.
132. Fan ST, Choi TK, Lo CM, Mok FP, Lai EC, Wong J. Treatment of hepatolithiasis: improvement of result by a systematic approach. Surgery 1991;109(4):474-80.
133. Beckingham IJ, Krige JE, Beningfield SJ, Bornman PC, Terblanche J. Subparietal hepaticojejunal access loop for the long-term management of intrahepatic stones. Br J Surg 1998;85(10):1360-3.
134. Faa G, Sciot R, Farci AM, Callea F, Ambu R, Congiu T, et al. Iron concentration and distribution in the newborn liver. Liver 1994;14(4):193-9.
135. Diaz G, Faa G, Farci AM, Balestrieri A, Liguori C, Costa V. Copper distribution within and between newborn livers. J Trace Elem Electrolytes Health Dis 1990;4(2):61-4.
136. Faa G, Nurchi V, Demelia L, Ambu R, Parodo G, Congiu T, et al. Uneven hepatic copper distribution in Wilson's disease. J Hepatol 1995;22(3):303-8.

9 PAPERS